Clim. Past, 16, 2055–2074, 2020
https://doi.org/10.5194/cp-16-2055-2020

Climate of the Past
Open Access
EGU

Early Jurassic climate and atmospheric CO_2 concentration in the Sichuan paleobasin, southwestern China

Xianghui Li[1], Jingyu Wang[1], Troy Rasbury[2], Min Zhou[1], Zhen Wei[1], and Chaokai Zhang[1]

[1]State Key Laboratory for Mineral Deposits Research, School of Earth Sciences and Engineering, Nanjing University, Nanjing, 210023, China
[2]Department of Geosciences, Stony Brook University, Stony Brook, NY 11794-2100, USA

Correspondence: Xiangui Li (leeschhui@126.com)

Received: 5 March 2020 – Discussion started: 13 May 2020
Revised: 3 September 2020 – Accepted: 14 September 2020 – Published: 4 November 2020

Abstract. Climatic oscillations have been developed through the (Early) Jurassic from marine sedimentary archives but remain unclear from terrestrial records. This work presents investigation of climate-sensitive sediments and carbon and oxygen isotope analyses of lacustrine and pedogenic carbonates for the Early Jurassic Ziliujing Formation taken from the Basin in southwestern China. Sedimentary and stable isotope proxies manifest that an overall secular (semi)arid climate dominated the Sichuan Basin during the Early Jurassic, except for the Hettangian. This climate pattern is similar to the arid climate in the Colorado Plateau region in western North America but is distinct from the relatively warm and humid climate in northern China and at high latitudes in the Southern Hemisphere. The estimated atmospheric CO_2 concentration (pCO_2) from carbon isotopes of pedogenic carbonates shows a range of 980–2610 ppmv (∼ 3.5–10 times the pre-industrial value) with a mean of 1660 ppmv. Three phases of pCO_2 (the Sinemurian 1500–2000 ppmv, the Pliensbachian 1000–1500 ppmv, and the early Toarcian 1094–2610 ppmv) and two events of pCO_2 rapidly falling by ∼ 1000–1300 ppmv are observed, illustrating the pCO_2 perturbation in the Early Jurassic. The perturbation of pCO_2 is compatible with seawater temperature and carbon cycle from the coeval marine sediments, suggesting a positive feedback of climate to pCO_2 through the Early Jurassic.

1 Introduction

Global paleotemperatures were possibly 5–10 °C higher than present during the Jurassic period based on climate modeling results (e.g., Rees et al., 1999; Sellwood and Valdes, 2008). However, seawater temperature fluctuated by −5 to +5 °C, or even much higher magnitude (e.g., Suan et al., 2008; Littler et al., 2010), based on estimates from the oxygen isotopes of the belemnite and bivalve fossils (Dera et al., 2011, and references therein). In the Sinemurian–Pliensbachian age, the mean sea surface temperatures of the North Atlantic were in excess of 28 °C (TEX_{86}), comparable with similar paleolatitudes during the Cretaceous and Early Cenozoic (Robinson et al., 2017), whereas in the late Pliensbachian age, the northern West Tethys Ocean (e.g., Paris basin, northern Spain basin) was ∼ 12.7 °C (e.g., Gómez et al., 2008; Gómez and Goy, 2011; Arabas et al., 2017), leading to a polar ice sheet hypothesis (e.g., Sellwood and Valdes, 2008; Suan et al., 2010; Dera et al., 2011; Gómez et al., 2016). At ∼ 183 Ma, during the early Toarcian oceanic anoxia event (T-OAE), the surface seawater temperature was high to ∼ 35 °C (e.g., Bailey et al., 2003; Korte et al., 2015), and a high temperature (plateau) even continued in the whole Toarcian (Dera et al., 2011). Examples of seawater temperature transitions between cold and hot show the climate oscillation through the Early Jurassic.

Data from the terrestrial realm also provide important details of environmental and climatic change (e.g., Hesselbo et al., 2000; Suan et al., 2010; Jenkyns, 2010; Philippe et al., 2017), from which the oscillated climate could be observed and revealed as well. Terrestrial proxies, such as flora

(e.g., Riding et al., 2013; Deng et al., 2017; Philippe et al., 2017), vegetation (Pole, 2009), and geochemistry (e.g., Riding et al., 2013; Kenny, 2015; Tramoy et al., 2016), as well as the atmospheric CO_2 concentration (pCO_2) record (e.g., Retallack, 2001a; Beerling and Royer, 2002; McElwain et al., 2005; Berner, 2006; Steinthorsdottir and Vajda, 2015), provide an emerging record of the Early Jurassic terrestrial climate and environment changes. Correspondingly, the proxy application of terrestrial sedimentary archives could play a key role in the global Early Jurassic correlation of the marine and terrestrial climate.

Proxies for pCO_2 are the important linkage between the marine and terrestrial climatic condition. Studies of the terrestrial pCO_2 record have focused on the Triassic–Jurassic boundary (e.g., Tanner et al., 2001; Cleveland et al., 2008; Schaller et al., 2011; Steinthorsdottir and Vajda, 2015) and the Toarcian oceanic anoxic event (McElwain et al., 2005), where pCO_2 estimates range from 1000 ppm to 4000 ppmv (e.g., Tanner et al., 2001; Cleveland et al., 2008; Schaller et al., 2011). Few relatively continuous pCO_2 records and coupled terrestrial climate changes have been documented for the Early Jurassic.

There are several large Triassic–Jurassic terrestrial basins in western China, in which the Sichuan Basin has a relatively complete and continuous continental sedimentary sequence of the Upper Triassic–Paleogene (e.g., SBGM, 1991, 1997; Wang et al., 2010). During the Early Jurassic, the Sichuan Basin was in the Boreotropical climate zone, a suggestion based on climate-sensitive sediments (Fig. 1a; Boucot et al., 2013), or a warm and temperate climate, suggested based on clay mineralogy and phytogeography (e.g., Dera et al., 2009). In this work, we present a field investigation, including lithofacies and paleosol interpretation, and carbon and oxygen isotope analyses of both lacustrine and pedogenic carbonates in the Sichuan Basin. New results allow us to reconstruct the paleoclimate and relatively consecutive pCO_2 record through the Early Jurassic, which we use to compare stable isotopes of marine sediments and estimated sea water temperature.

2 Geological setting and stratigraphy

Southwestern China, including the provinces of Yunnan, Sichuan, Chongqing, and Guizhou, had been the main part of the upper Yangtze Plate since the Proterozoic and possibly since the Neoarchean. With the amalgamation of the Cathaysia and Yangtze plates, it became the western South China plate or cratonic basin since the Neoproterozoic (Sinian) and continued to the late Middle Triassic. Via the Indosinian orogeny, new foreland basins were formed since the Late Triassic (e.g., He and Liao, 1985; Li et al., 2003), recording the Mesozoic and Cenozoic evolution of tectonics, environment, and climate in southwestern China.

The Mesozoic Sichuan paleobasin was confined by the Longmenshan thrust belt in the northwest, the Micangshan–Dabashan arcuate thrust belt in the northeast (Fig. 1b), and the northern hilly topography boundary of the Yunnan–Guizhou plateau in the south and east. It was mainly developed during the Late Triassic–Jurassic and includes provincial areas of eastern Sichuan, northern Guizhou, western Hubei, northwestern Hunan, and the entirety of Chongqing. This Triassic–Jurassic Sichuan foreland basin was much larger than the present Sichuan Basin in eastern Sichuan province. We estimate the size of the Sichuan paleobasin is roughly 480 000 km^2 based on lithofacies paleogeography (Fig. 1b; Ma et al., 2009; Li and He, 2014) and suggest naming this the grand Sichuan paleobasin (GSB).

The Mesozoic terrestrial sediments accumulated up to $\sim$ 9 km (Guo et al., 1996) in the GSB, and the Jurassic part can be up to 3–3.5 km thick (SBGM, 1991). Two types of Lower Jurassic deposits have been distinguished (Table 1): the Baitianba Formation (Fm) in the north ($\sim$ 10 %) and the Ziliujing Fm (e.g., SBGM, 1991; Wang et al., 2010) in the south (over 90 % of the basin).

The Baitianba Fm was deposited unconformably on the Upper Triassic Xujiahe Fm and is overlain conformably by the Middle Jurassic Xintiangou Fm and Qianfoyan Fm (Table 1). It is mainly composed of grayish shales and sandstones with coal layers and massive conglomerates. Abundant plant fossils, sporopollens, conchostracans, bivalves, and gastropods indicate it is of the Early Jurassic (SBGM, 1991, 1997). Sporopollen assemblages of the Hettangian–Sinemurian age were found in the lower part (Zhang and Meng, 1987) and the Pliensbachian–Toarcian assemblages were reported in the upper part (Wang et al., 2010).

The Ziliujing Fm is composed of variegated and reddish mudrocks (some shales) intercalated with sandstones, siltstones, and bioclastic limestones, as well as dolomitic marlstones and limy dolomites, conformably or unconformably overlying the Xujiahe Fm or Luqiao Fm and conformably underlying the Xintiangou Fm (SBGM, 1997; Table 1). It has been dated to the Early Jurassic by fossil assemblages of bivalves, ostracods, conchostracans, and plants. Dinosaur fauna can be well correlated to the Lufeng Fauna in central Yunnan (e.g., Dong, 1984; SBGM, 1991, 1997; Peng, 2009). This formation is subdivided into five parts in ascending order: the Qijiang, Zhenzhuchong, Dongyuemiao, Ma'anshan, and Da'anzhai members (SBGM, 1997; Table 1). Of these, the former two are sometimes combined as the Zhenzhuchong Fm (e.g., SBGM, 1991; Wang et al., 2010).

The Da'anzhai Member is characterized by dark gray to black shales and bioclastic limestones with a southward increase of reddish mudrocks (SBGM, 1991, 1997; Wang et al., 2010) and is regarded as the sediment in a grand Sichuan paleolake (e.g., Ma et al., 2009; Li and He, 2014). Ostracod assemblages indicate it is the late Early Jurassic (e.g., Wei, 1982; Wang et al., 2010). A Re-Os isochron age of 180.3 ± 3.2 Ma associated with an organic carbon isotope

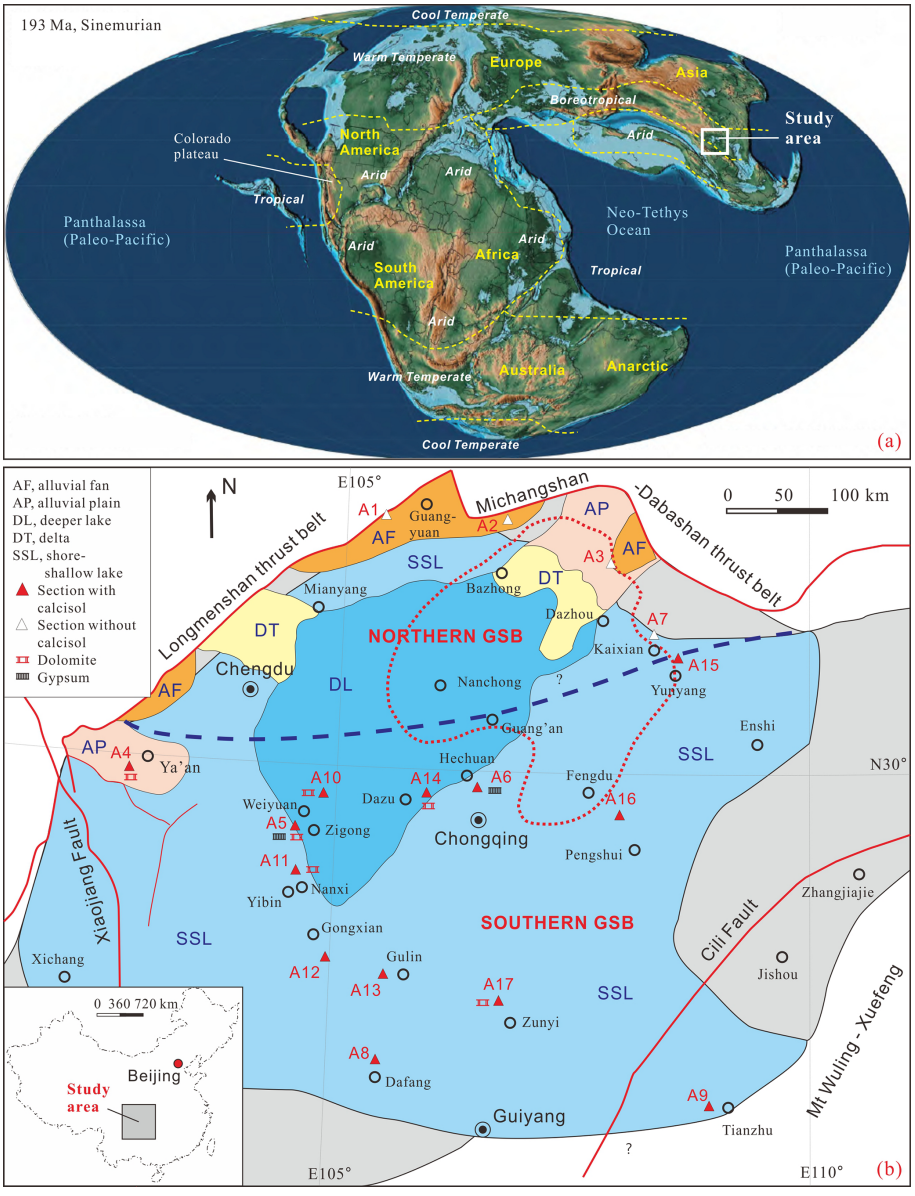

Figure 1. **(a)** Global Early to Middle Jurassic climate zones (Boucot et al., 2013) laid over an Early Jurassic (~ 193 Ma, Sinemurian) paleogeographic map (Scotese, 2014). **(b)** Lithofacies paleogeographic sketch of the grand Sichuan paleobasin (GSB) in the early Early Jurassic (Zhenzhuchong and Dongyuemiao members) showing locations of the observed and analyzed sections and climate-sensitive sediments. The lithofacies paleogeographic map was composed and modified from Ma et al. (2009) and Li and He (2014). The blue area is the extent of the paleolake, estimated as ~ 380 000 km^2. The blue-gray region is the basin shape, estimated as ~ 480 000 km^2. The dotted red line encircles the deeper lake area in the late Early Jurassic (Ma'anshan and Da'anzhai members). The black dashed line is the northern edge of Calcisol occurrence, which may separate the climate of the GSB into the northern and southern types. Triangles with numbers are locations of observed and analyzed sections: A1, Xiasi section, Jian'ge; A2, Puji section, Wangcang; A3, Shiguansi section, Wanyuan; A4, Shaping section, Ya'an (bed and thickness from Wen and Zhao, 2010); A6, Tanba and Maliuping section, Hechuan (bed and thickness from Wang et al., 2010); A7, Wenquan section, Kaixian (thickness from Wang et al., 2010). The location and source data of sections A5 and A8–A17 (climate-sensitive sediments) refer to Supplement Table S1.

Table 1. Stratigraphic framework of the Lower Jurassic Ziliujing Fm in Sichuan and adjacent area (GSB), southwestern China.

Epoch	Age	Formation	W Sichuan (Ya'an)	E Sichuan and Chongqing	S Sichuan and N Guizhou	N Sichuan
Middle Jurassic	Aalenian	Xintiangou Fm	Xintiangou Fm	Xintiangou Fm	Xintiangou Fm	Qianfoyan / Xintiangou Fm
Early Jurassic	Toarcian	Ziliujing Fm	Da'anzhai Mem (Bed 20-34)	Da'anzhai Mem	Da'anzhai Mem	Baitianba Fm
	Pliensbachian		Ma'anshan Mem (Bed 9-18)	Ma'anshan Mem	Ma'anshan Mem	
	Sinemurian		Dongyuemiao Mem (Bed 8)	Dongyuemiao Mem	Dongyuemiao Mem	
			Zhenzhuchong Mem (Bed 1-7)	Zhenzhuchong Mem	Zhenzhuchong Mem	
	Hettangian		**Hiatus**	Qijiang Mem	Qijiang Mem	?
Late Triassic	Rhaetian	Xujiahe Fm	Xujiahe Fm	Xujiahe Fm	Xujiahe Fm	Xujiahe Fm

Stratigraphic classification and correlation were composed from Dong (1984), SBGM (1997), Wang et al. (2010), Wen and Zhao (2010), and Xu et al (2017). Re-Os isotope age of the lower Da'anzhai Member is 180.3 ± 3.2 Ma in western Sichuan (Xu et al., 2017) (Fm stands for Formation; Mem stands for Member).

excursion indicates that the lower Da'anzhai Member corresponds to the T-OAE (Xu et al., 2017).

The Ma'anshan Member is comprised of violet and red mudrocks with a few greyish and greenish thin-bedded fine sandstones and siltstones in which floral fossils are common (Li and Meng, 2003). The Dongyuemiao Member consists of greenish and reddish mudrocks and siltstones with greyish bioclastic limestone and marlstone, of which abundant bivalve and plant fossils were reported from eastern Sichuan and Chongqing (Li and Meng, 2003; Meng et al., 2003; Wang et al., 2010). The Zhenzhuchong Member is dominated by violet red mudrocks and shales intercalated with thin-bedded sandstones and/or siltstones and numerous plant fossils of the Early Jurassic affinity (e.g., Duan and Chen, 1982; Ye et al., 1986). Taken together, fossil associations suggest that the three members were deposited in the middle to late Early Jurassic. The age limitation of the overlying Da'anzhai Member and the correlation to the Lufeng dinosaur fauna places these members in the Sinemurian–Pliensbachian, and the Zhenzhuchong and Dongyuemiao Fms are suggested to be from the Sinemurian (Table 1).

The Qijiang Member is composed of quartz arenite interbedded and intercalated with dark shales. Coal seams are often seen in the middle of the Qijiang Member. This member mainly occurs in the central part of the GSB. It is likely the earliest Jurassic, possibly Hettangian age, but plant fossils cannot precisely indicate the age (Wang et al., 2010).

3 Materials and methods

We have measured sections and made detailed observations and descriptions of sedimentary characteristics for lithofacies analysis at six outcrop sections (Locations A1–A4, A6, and A7, Fig. 1). Published descriptions for other sections (Locations A5, A8, and A9, Fig. 1) are integrated into our observations. Details of microscopic examination of sedimentary rocks and analysis of sedimentary facies underpinning the climate analysis are attached as the Supplement Note S1. Below we state climate-sensitive sediment observations, carbon and oxygen isotope analyses, and estimates of pCO_2.

3.1 Observation of climate-sensitive sediments

Climate-sensitive sediments are mainly dolomites, gypsum, and paleosols, which are used to analyze the climate in this work (Table S1).

Dolomites and gypsum are relatively easy to recognize both in the field and under a microscope. We distinguish dolomites from limestones following Tucker (2011) and Flügel (2004). As Flügel (2004) stated, field distinctions of limestone and dolomite can also be made, although detailed differentiation of carbonate rocks is best performed in the laboratory. In the field, we recognize gypsum via particular structures, such as a chicken-wire cage, gypsum pseudomorph, and clusters of (0.5–1 cm) pore.

There are multiple classifications of paleosols (e.g., Wright, 1992; Mack et al., 1993; Retallack, 2001b; Imbellone, 2011), mostly based on the US Soil Taxonomy. We recognized paleosols in the field based on color, structures, horizonation, root traces, and textures, and followed the general classification paleosols by Mack et al. (1993) and Retallack (2001b). In this paper, paleosols are described following the procedures of the Soil Survey Manual and classified according to Soil Survey Staff (1998).

Within the measured and observed sections, paleosol profiles were mainly identified from the two main sections A4 and A6 (Figs. S1 and S2, and Table S2). Horizonation, Bk horizon thickness, boundaries, structures, trace fossils, rootlets, carbonate accumulations (calcretes), etc. were recorded (Table S2). Paleosols interpreted in other cited sections (Fig. 1) rely on the description of lithology, structure, and calcrete in the original references. Based upon a modification of the Retallack (1998) categorization of paleosol

maturity, the relative paleosol development (maturity) was assigned.

3.2 Analyses of carbon and oxygen isotopes

The 10 lacustrine carbonate samples were analyzed for carbon and oxygen isotopes from the Da'anzhai Member at the Shaping section, Ya'an (Location A4; Fig. S1 and Table S3). A total of 26 pedogenic carbonate samples were analyzed for carbon and oxygen isotopes from 32 paleosols of the Ziliujing Fm at the same section (Fig. S1 and Table S4). Two or three microdrilling powder samples (columns 7 and 8 in Table S4) were taken from the same individual calcrete for stable isotope analysis, and then a mean value for each calcrete sample was calculated (columns 9 and 10 in Table S4).

At the field scale, calcretes are ginger-like and sporadically spaced within the soil horizon. We observed no linear and planar calcretes that would indicate precipitation at or below the water table. Before drilling, thin sections were petrographically studied using polarized light microscopy and cathodoluminescence imaging. Micritic calcite is predominant in both lacustrine and pedogenic carbonate samples, with no evidence for carbonate detritus in calcretes (Fig. 2a and b). The micritic calcites used for stable isotope analyses are chiefly null- to non-luminescent, with $<10\,\%$ light orange and brownish luminescence, indicating genesis primarily in the vadose zone. While luminescent calcretes indicate a high possibility of hydrological influence (e.g., Mintz, et al., 2011), we sampled to avoid this. Based on petrography and cathodoluminescence (CL) imaging together with the field observations, the dense micritic zones sampled for the stable isotope composition should give pristine $\delta^{13}C$ values that can be used to estimate pCO_2.

Microsampling of lacustrine and pedogenic carbonates focused on only micrites, avoiding diagenetic spar from cracks, veins, and vug spaces. Powder samples were obtained using a dental drill (aiguille diameter $\phi = 1$–2 mm).

Isotopic analyses were conducted on 0.3–0.5 mg powder samples. Powder samples were dried in an oven at 60 °C for 10 h before being moved to the instrument. Carbon dioxide for isotopic analysis was released using orthophosphoric acid at 70 °C and analyzed online in a DELTA-Plus XP (CF-IRMS) mass spectrometer at the State Key Laboratory for Mineral Deposits Research, Nanjing University. The precision of the measurements was regularly checked with a Chinese national carbonate standard (GBW04405) and the international standard (NBS19) and the standard deviation of $\delta^{13}C$ was $\pm 0.1\,‰$ over the period of analysis. Calibration to the international Pee Dee Belemnite (PDB) scale was performed using NBS19 and NBS18 standards.

3.3 Calculation of atmospheric CO_2 concentration

The Cerling (1991, 1999) equation was used to calculate the pCO_2 using the carbon isotope of pedogenic carbonates as below:

$$C_a = S_{(z)}(\delta^{13}C_s - 1.0044\delta^{13}C_r - 4.4)/(\delta^{13}C_a - \delta^{13}C_s), \quad (1)$$

where C_a is pCO_2; $\delta^{13}C_s$, $\delta^{13}C_r$, and $\delta^{13}C_a$ are the isotopic compositions (‰) of soil CO_2, soil-respired CO_2, and atmospheric CO_2, respectively; and $S_{(z)}$ is the CO_2 contributed by soil respiration (ppmv).

$\delta^{13}C_s$ is often calibrated by fractionation factor $-8.98\,‰$ with the formula $-8.98\,‰ + \delta^{13}C_c$ (Ekart et al., 1999), with which $\delta^{13}C_c$ is the measured result of pedogenic calcrete. Alternatively, $\delta^{13}C_s$ can be replaced by $\delta^{13}C_{sc}$, which is calibrated by carbon isotope ratio of pedogenic carbonate at 25 °C based on latitude–temperature correlations (Besse and Courtillot, 1988; Ekart et al., 1999) following the equation $\delta^{13}C_{sc} = (\delta^{13}C_c + 1000)/((11.98 - 0.12 \times T)/1000 + 1) - 1000$ (Romanek et al., 1992). We used both $\delta^{13}C_s$ and $\delta^{13}C_{sc}$ to calculate the pCO_2 (Table S4).

The value of $\delta^{13}C_r$ represents the carbon isotope ratio of average bulk C3 vascular tissue (Arens et al., 2000), reflecting atmospheric $\delta^{13}C$ (Jahren et al., 2008). The $\delta^{13}C_{om}$ of organic matter within paleosols based on the range of modern C3 ecosystem fractionations (Buchmann et al., 1998; Ekart et al., 1999) is commonly used for $\delta^{13}C_r$. However, the $\delta^{13}C_r$ could be compromised in fossil soils due to oxidation and metabolism of organic matter after burial (Nadelhofer and Fry, 1988). In this paper, we use the $\delta^{13}C_{om}$ from the Paris Basin (Bougeault et al., 2017; Peti et al., 2017) for the Sinemurian–Pliensbachian $\delta^{13}C_r$ and from Cardigan Bay, UK (Xu et al., 2018), for the Toarcian.

The $\delta^{13}C_a$ value, the carbon isotopic composition of the atmosphere, was about $-8\,‰$ in the 1980s, being depleted relative to the pre-industrial atmosphere, which was around $-6.5\,‰$ (Friedli et al., 1986). The average value of $-6.5\,‰$ has been chosen as the $\delta^{13}C_a$ for acquiring $\delta^{13}C_r$ and $S_{(z)}$ (e.g., Ekart et al., 1999; Robinson et al., 2002), and the $\delta^{13}C_a$ was generally calibrated as $\delta^{13}C_{ac}$ from $\delta^{13}C_r$ using the formula $(\delta^{13}C_r + 18.67)/1.1$ (Arens et al., 2000). Herein we used both calibrations to calculate the $\delta^{13}C_a$ (Table S4).

$S_{(z)}$ is the largest source of uncertainty in pCO_2 estimates (Breecker, 2013) and the uncertainty arises primarily from the sensitivity to soil-respired CO_2 ($S_{(z)}$ (Montañez, 2013). It is a function of depth and effectively constant below 50 cm (e.g., Cerling, 1991). $S_{(z)} = 2500$ ppmv is suggested for the subhumid temperate and tropical climates (Breecker et al., 2010), 2500–5000 ppmv is suggested for higher moisture and productivity soil (Montañez, 2013), 2000 ppmv is suggested for semi-arid areas (Breecker et al., 2009), 1500–2000 ppmv is suggested for aridisols and alfisols (calcisol-argillisol), and 2000 ± 1000 is suggested for paleo-vertisol (Montañez, 2013), with 1000 ppmv in desert areas (Breecker et al., 2010) or 400 ± 200 ppmv for immature soil (Montañez, 2013). In this context, we chose the $S_{(z)} = 2000$ ppmv for calculating pCO_2 at 25 °C as the calcisols are reddish-brownish aridisols, and we also compared the results with that by $S_{(z)} = 2500$ ppmv (Table S4). Additionally, we took

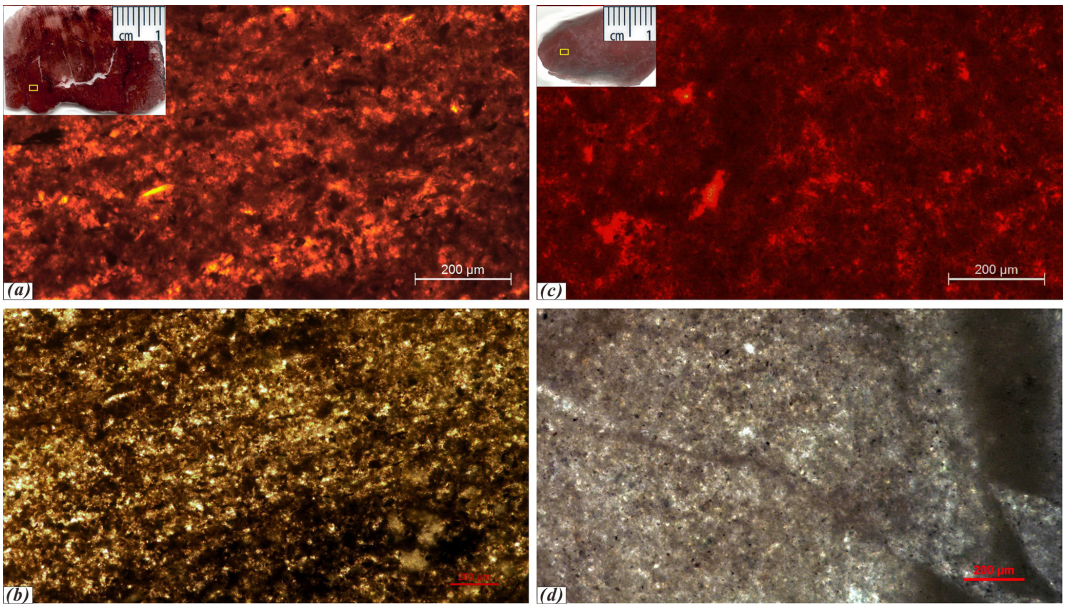

Figure 2. Microscopic cathodoluminescence and polarized light photos of representative calcrete samples from the Ziliujing Fm at the Shaping section, Ya'an: **(a)** and **(b)** Sample J1z-12-01, Bed B12, Ma'anshan Member; **(c)** and **(d)** Sample J1z-22-01, Bed B22, Da'anzhai Member. Pedogenic calcites are mainly null to non-luminescent, minor are orange and red luminescence. Inserts are the scanned photos of thin section, and rectangles are the area under cathodoluminescence and drilling.

samples at the middle and lower Bk horizon (often $> \sim 20$–30 cm to the Bk top). This means that the depth of calcrete samples in the examined paleosols was generally deeper than 50 cm below the paleosol surface, meeting the requirement for a constant value of $S_{(z)}$.

4 Results

Based on the investigation of cross sections (locations A1–A4, and A6–A7; Fig. 1), we have classified six sedimentary facies units in the Ziliujing Fm. They are alluvial fan, fluvial river, floodplain, lake, lake delta, and swamp facies. Details of description and interpretation are in the Supplement Note S1. Below are results of climate-sensitive sediment observation, stable isotope analyses, and pCO_2 calculation.

4.1 Climate-sensitive sediments

Field observation combined with published calcrete materials shows that paleosols widely occur in the Lower Jurassic Ziliujing Fm of the GSB (Figs. 1, 3, and 4). A total of 32 paleosols were observed and described at the Shaping section, Ya'an, and five paleosols were found at the Tanba section, Hechuan (Table S2).

Most of paleosols are reddish (GSA Munsell Rock Color 5R 2/2, 5R 3/4, 5R 4/2) and brownish (10R 3/4, 10R 5/4) (Fig. 3 and Table S2). Beds of paleosols are mainly angular and subangular, and a few are prismatic and platy. Slickensides are common. Mottles (Fig. 3a), rootlets and rhizoliths (Fig. 3c), and burrows sometimes occur with strong leaching structures (Fig. 3a). Occasionally mudcracks are associated with the aforementioned structures (Fig. 3d).

All paleosols are calcic, with more or less calcretes in Bk horizons. The thickness of Bk horizons mainly changes from 30 and 100 cm, and it partly changes up to 170 cm (Table S2). Calcretes are generally ginger-like, ellipsoid, sub-globular, and irregular in shape (Fig. 3b and e), and nodules are 1–3 cm and even up to 8–15 cm (paleosols J1z-10-01 and J1z-12-01) in size (Fig. 3e). Calcrete is often less than 0.5 %–1 % in an individual paleosol, but a few can be up to 3 %–5 % (paleosol J1z-3-01; Fig. 3b) and even 10 % (paleosols J1z-5-02 and 18HC-10).

All of the above paleosols are defined as relatively mature calcisols (Mack et al., 1993), a kind of aridisol (Soil Survey Staff, 1998; Retallack, 2001b). The original lithofacies were chiefly argillaceous and silty (split-fan) overbank, interchannel, and floodplain deposits (Figs. S1 and S2). Some formed landward of the paleo-lakeshore.

Dolomites were found at seven locations in the central and southern GSB (Figs. 1, 4, and Table S1). The dolomites chiefly occur in the Toarcian Da'anzhai Member and a few in the Sinemurian–Pliensbachian Dongyuemiao and Ma'anshan members (Fig. 4). They are often massive whitish (Figs. 3f and S3e) and micritic (Fig. S4b and d), likely indicating an authigenic origin.

Gypsum is recorded in two locations (Figs. 1, 4, and Table S1). One is located at Zigong (Location A5; SBG, 1980). The other lies at Hechuan (Location A6), which can be iden-

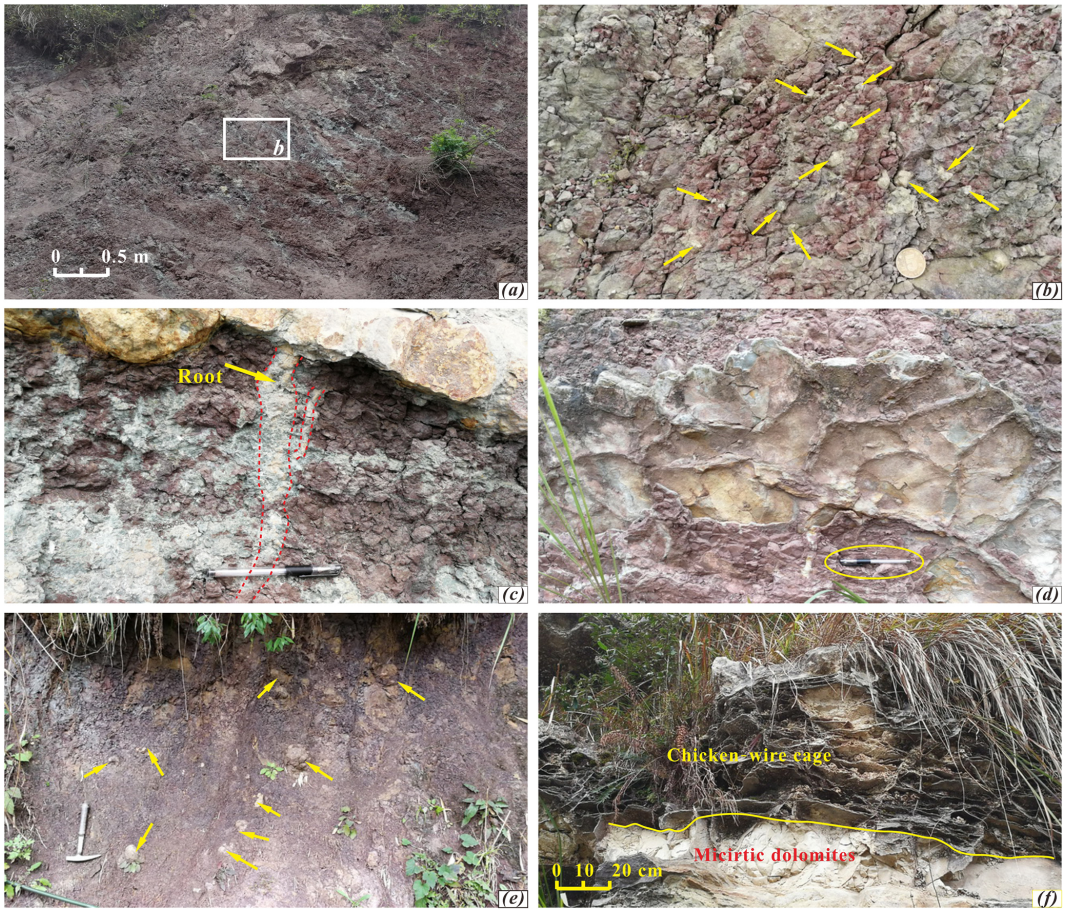

Figure 3. Field photographs of climate-sensitive sediments from the Lower Jurassic Ziliujing Fm in the GSB. **(a)** Reddish purple calcisol with strong leaching structure from lower Bed H8 of the upper Ma'anshan Member at Tanba, Hechuan. **(b)** Reddish purple calcisol showing the density and size of calcretes. The horizon and location are the same as **(a)**. Arrows point to calcretes. The coin is 2.0 cm in diameter. **(c)** Reddish purple calcisol with strong leaching structure and rhizoliths from Bed H13 of the top Ma'anshan Member at Maliuping, Hechuna. The pen is 15 cm long. **(d)** Mudcracks from lower Bed H8 of the upper Ma'anshan Member at Maliuping, Hechuan. The pen is 15 cm long. **(e)** Brownish red calcisol with big calcretes (calcareous concretions). Arrows point to big calcretes. Calcisol horizon J1z-10-01 from Bed B10 of the Ma'anshan Member at Shaping, Ya'an. The hammer is 34 cm long. **(f)** Chicken-wire cage structure from Bed H12 of the Da'anzhai Member at Maliuping, Hechuan.

tified by chicken-wire cage structure and is associated with micritic dolomites (Fig. 3f).

4.2 Carbon and oxygen isotope values

The $\delta^{13}C$ values of lacustrine carbonate samples range from $-2.02\,‰$ to $-4.07\,‰$, and $\delta^{18}O$ values range from $-9.91\,‰$ to $-12.28\,‰$ (Table S3 and Fig. 5). An increasing trend of both carbon and oxygen isotope ratios is observed from lower to upper horizons across a 45 m stratal interval of the lower Da'anzhai Member (Fig. 6).

Pedogenic carbonate samples have $\delta^{13}C$ values from $-3.52\,‰$ to $-8.10\,‰$, which fall in the typical stable isotope range for pedogenic carbonates. Values of $-6\,‰$ to $-8.0\,‰$ characterize the sequence of the Zhenzhuchong Member and the main Ma'anshan Member, with an abrupt increase to $-5.5\,‰$ to $-3.5\,‰$ at the top of the Ma'anshan Member (samples J1z-16-01 and J1z-18-01; Fig. 6). The $\delta^{18}O$ values are mainly from $-11.3\,‰$ to $-13.10\,‰$ in the interval of the Zhenzhuchong Member and Ma'anshan Member. The $\delta^{18}O$ follows $\delta^{13}C$ with a sudden increase to $-5.5\,‰$ at the top of the Ma'anshan Member (Fig. 6). Large and frequent variations of both carbon and oxygen isotope ratios can be observed in the lower Da'anzhai Member (Fig. 6 and Table S4).

4.3 CO_2 concentrations

pCO_2 values based on paleobarometer modeling of paleosol calcite (Cerling, 1999) vary depending on the parameters used for the calculation.

If $S_{(z)} = 2500$ ppmv and $\delta^{13}C_a = -6.5\,‰$ (constant pre-industrial atmosphere), pCO_2 values range between ~ 1140

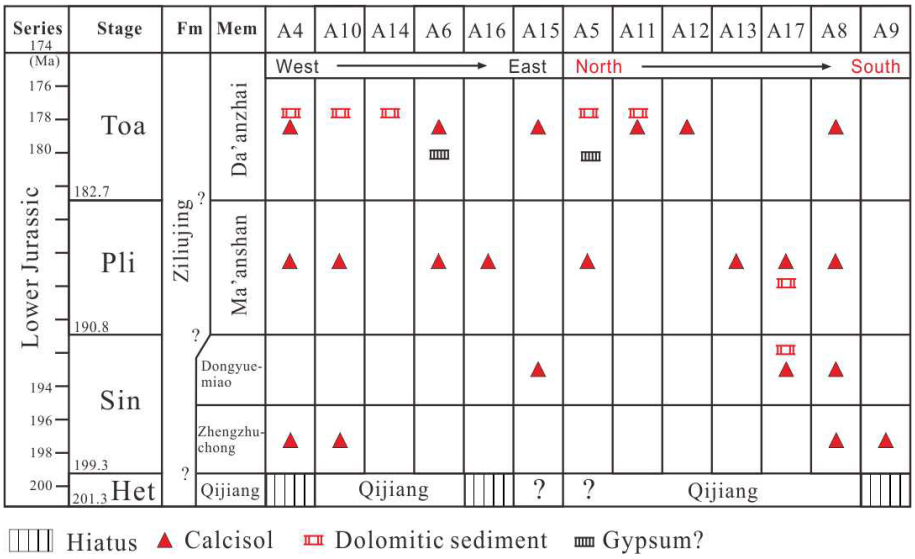

Figure 4. Diagram showing the temporal and spatial variation of climate-sensitive sediments in GSB. Section locations and data sources refer to Table S1.

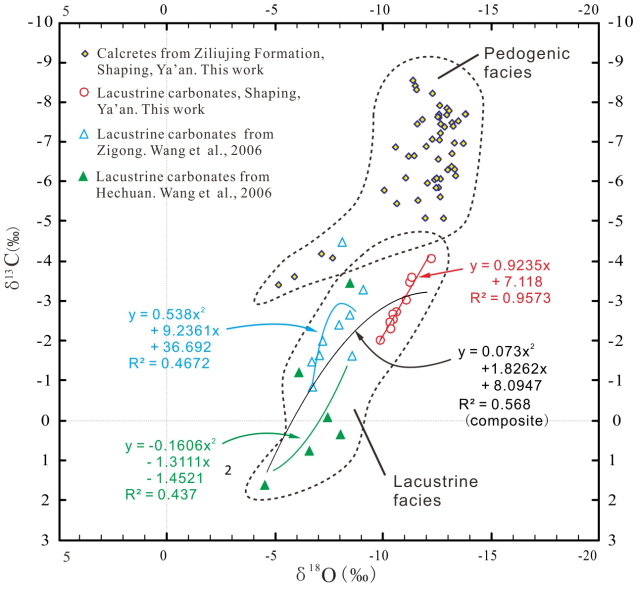

Figure 5. A cross-plot and the covariance of carbon and oxygen isotopic values of the Lower Jurassic pedogenic and lacustrine carbonates from the GSB. Note the pronounced covariance ($R^2 = 0.957$) between $\delta^{13}C$ and $\delta^{18}O$ from the Shaping section, Ya'an, indicating a compositional arid evaporate and closed pattern lake, and also note the moderate covariance ($R^2 = 0.47$ and 0.44) between $\delta^{13}C$ and $\delta^{18}O$ from Zigong and Hechuan, indicating a (semi)arid and semi-closed pattern lake.

and ~3460 ppmv with a mean of 1870 ppmv (column 15 in Table S4), and when $S_{(z)} = 2500$ ppmv and $\delta^{13}C_a = (\delta^{13}C_r + 18.67)/1.1$, pCO_2 values change between ~1230 and ~3260 ppmv with a mean of 2070 ppmv (column 16 in Table S4).

When $S_{(z)} = 2000$ ppmv and $\delta^{13}C_s = -8.98 + \delta^{13}C_c$ are used, pCO_2 values are ~940–2530 ppmv with a mean 1600 ppmv (column 17 in Table S4), and if $S_{(z)} = 2000$ ppmv and $\delta^{13}C_s = (\delta^{13}C_c + 1000)/((11.98 - 0.12 \times 25)/1000 + 1) - 1000$ are adopted, pCO_2 values become ~980 to ~2610 ppmv with a mean 1660 ppmv (column 18 in Table S4). Details of the different parameters and pCO_2 results can be seen in Table S4.

Results show that pCO_2 values at $S_{(z)} = 2500$ ppmv are larger than at $S_{(z)} = 2000$ ppmv and that the $S_{(z)}$ is the largest uncertainty leading to different pCO_2 values. The highest difference (columns 16 and 18 in Table S4) of pCO_2 is ~650 ppmv (3260 − 2610 ppmv) (Sample J1z-22-01 at depth 324.5 m), while the lowest difference is ~245 ppmv (1226−981 ppmv) (Sample J1z-12-01 at depth 148.9 m), and the mean is ~370 ppmv. In addition, when $S_{(z)}$ is the same, the pCO_2 values are close even if other parameters are different (comparison between columns 15 and 16 and 17 and 18 in Table S4; Fig. 6).

Whatever parameters are used, the trend of pCO_2 over the epoch is quite similar (Fig. 6). We chose $S_{(z)} = 2000$ ppmv (column 18 in Table S4) to illustrate the nature of the Early Jurassic pCO_2 in the GSB.

pCO_2 values mostly range between 980 and 2610 ppmv, and the mean 1660 ppmv is ~6 times the pre-industrial 275 ppmv. Most of the pCO_2 values are 1000–2000 ppmv, with the mean 1580 ppmv in the Zhenzhuchong and

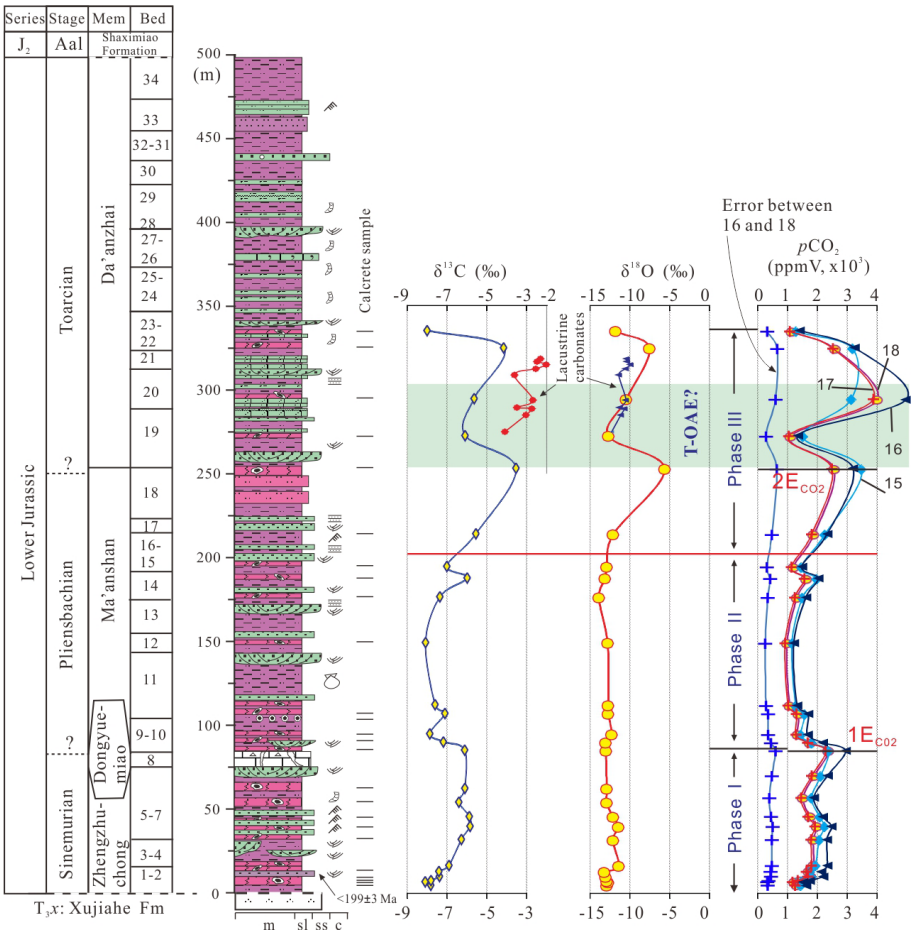

Figure 6. Diagram of the Lower Jurassic strata and lithological log at the Shaping section, Ya'an, with carbon and oxygen isotope values of pedogenic and lacustrine carbonates and the pCO_2 curve. Three phases and two events can be observed for both stable isotope values of pedogenic carbonates and pCO_2 estimate. A legend of lithology in log refers to Supplement Figs. S1 and S2. T-OAE stands for the Toarcian oceanic anoxic event. The $1E_{CO_2}$ and $2E_{CO_2}$ are events of rapid falling pCO_2. Numbers 15 to 18 are the curves of pCO_2 in different parameters, and details refer to Supplement Table S4. Discrepancies (errors) are produced from the pCO_2 subtraction of column 16 ($S_{(z)}$ =2500 ppmv) from column 18 ($S_{(z)}$ = 2000 ppmv) in Table S4, indicating that the largest uncertainty for the estimate of pCO_2 is the $S_{(z)}$. The highest difference (columns 16 and 18 in Table S4) of pCO_2 is 652 ppmv (3262 − 2610 ppmv) (Sample J1z-22-01 at depth 324.5 m), the lowest difference is 245 ppmv (1226 − 981 ppmv) (Sample J1z-12-01 at depth 148.9 m), and the mean is ∼ 370 ppmv.

Ma'anshan members being ∼ 3.5–7.5 times the pre-industrial pCO_2 value.

It is noted that the Gaussian errors of pCO_2 range from 384 to 1017 ppmv with a mean 647 ppmv (Table S5), leading to a large uncertainty of the mean ∼ 39 %. The largest source of the uncertainty is the standard error (766 ppmv) of modern soil carbonate (Breecker and Retallack, 2014). The pCO_2 uncertainty decreases by ∼ 20 % if half (383 ppmv) of the standard error of soil carbonate is selected, and decreases to ∼ 12 % if 0.25 (∼ 191 ppmv) standard error is used. The second largest source of error in the pCO_2 is the $S_{(z)}$ estimate. The uncertainty of pCO_2 becomes much smaller when the $S_{(z)}$ is larger, e.g., it will fall from ∼ 39 % to ∼ 17 % if $S_{(z)}$ = 5000 ppmv instead of 2000 ppmv. Other parameters such as temperature, $\delta^{13}C_r$, $\delta^{13}C_a$, and $\delta^{13}C_s$ contribute very little to the calculated pCO_2 uncertainty. The uncertainty of pCO_2 is the same when $\delta^{13}C_a$ is determined by the transfer from $\delta^{13}C_c$ of marine planktonic fossil carbonates (Table S8) or from organic matter (Table S5).

5 Discussion

The Jurassic marine record shows climatic and environmental oscillations (e.g., van de Schootbrugge et al., 2005; Dera et al., 2011; Gómez et al., 2016; Arabas et al., 2017), including sea water temperature fluctuation and carbon cycle reorganization recorded in both carbonate and organic matter. The climate changes and events recorded in the marine realm have been mainly attributed to Karoo–Ferrar volcanism (e.g., Hesselbo et al., 2000; Caruthers et a., 2013),

sea level change (e.g., Hesselbo and Jenkyns, 1998; Hallam and Wignall, 1999), orbital forcing (e.g., Kemp et al., 2005; Huang and Hesselbo, 2014; Storm et al., 2020), and/or the opening of the Hispanic corridor (e.g., van de Schootbrugge et al., 2005; Arias, 2009). Eruption of the Karoo–Ferrar and Central Atlantic magma is thought to have released large amounts of CO_2 into the atmosphere in a short amount of time, resulting in rising temperatures of both marine and continental realms. The nearly continuous record of the Jurassic strata in the GSB provides an excellent test of this hypothesis in the terrestrial realm. We compare the climate and pCO_2 record from the GSB in relationship to the marine temperature records.

5.1 Paleoclimate variation

During the Late Triassic, southwestern China was warm to hot and humid and occupied a tropical and/or subtropical zone, as demonstrated by palynoflora, coals, and perennial riverine and lacustrine lithofacies in the Xujiahe Fm (e.g., Huang, 1995; Li et al., 2016). However, the climate became dry through the Early Jurassic, manifesting as climate-sensitive sediments and stable isotopes, although there are two lithofacies packages reflecting two major lake stages (for details refer to the Supplement Note S1) in the GSB.

5.1.1 The Hettangian age

In the Hettangian, the climate was warm and humid like the Late Triassic in the GSB. The Qijiang Member is comprised of mainly mature quartz arenites and siltstones with coals (Fig. 7), as well as siderite concretions, indicating a stable tectonic setting and warm and humid climate in the eastern and southern GSB. Climate was similar across the whole region, because multiple coal layers occur in the lower Baitianba Fm. The alluvial fan system of the lower Baitianba Fm (Figs. 7 and S6) is characterized by moderate to good roundness and sorting of gravels with sandy matrix (Fig. S3a; e.g., Liu et al., 2016; Qian et al., 2016; and this work). In the Newark basin of eastern North America, climate-sensitive sediments such as nodules of carbonate and gypsum (pseudomorph), as well as mudcrack in mudflat facies, indicate an arid climate in the fifth cycle of the Hettangian ($>$ 199 Ma) Passaic Fm (Kent et al., 2017). The more widespread eolian Navajo Sandstone, dated as Hettangian–Sinemurian (200–195 Ma; Parrish et al., 2019), indicates arid in the Colorado Plateau (Fig. 1a; Boucot et al., 2013).

5.1.2 The Sinemurian age

The early Sinemurian Zhenzhuchong Member is a combination of riverine floodplain and lacustrine facies (Supplement Note S1). The lithology is dominated by violet red mudrocks with few thin greyish and greenish fine sandstones and siltstones. The reddish color of the rocks may indicate a change of climate. Differences in the color appearance show that the reddish color started in the middle member in the central basin (Location A6; Fig. S2) but almost developed through the whole member in the western basin (Location A4; Fig. 6).

Within reddish mudrocks of the floodplain facies, multiple calcisols were observed at the Shaping section, Ya'an (Location A4; Figs. 1, 4, and 7), including a strongly leached calcisol horizon (Fig. S3c). We also interpret the reddish muddy sediments with abundant calcretes as the calcisol at sections of Dafang (Location A8; Zhang et al., 2016), Tianzhu (Location A9; Li and Chen, 2010), and Weiyuan (Location A10; SBG, 1980). The calcisols indicate a (semi)arid climate in the Sinemurian.

This climate change, interpreted from reddish mudrocks and paleosols, is consistent with the floral fossils (e.g., Huang, 2001; Wang et al., 2010), suggesting the decreasing humidity and increasing temperature from the Late Triassic epoch and the Hettangian age into the Sinemurian age in the southern GSB. However, in the northern GSB there are few proxies for climate change, and alluvial fan and lacustrine delta facies common in the middle Baitianba Fm (Fig. S6; e.g., Qian et al., 2016) do not give us information on climate.

The late Sinemurian Dongyuemiao Member also has reddish mudrocks and calcisols, similar to the Zhenzhuchong Member. Pedogenic calcretes were reported at Dafang (Location A8; Zhang et al., 2016), Tianzhu (Location A9; Li and Chen, 2010), and Yunyang (Location A15; Meng et al., 2005) and in the central and southern GSB (Figs. 4 and 7 and Table S2), indicating continued arid climate conditions at the time.

The Sinemurian (semi)arid climate interpreted from reddish mudrocks and calcisols is supported by the flora (Li and Meng, 2003) and the mudrock geochemistry (Guo et al., 2017). Few records of coeval terrestrial climate are documented from other continents or regions in the literature. The Whitmore Point Member of the Moenave Fm deposited in dryland lakes (Tanner and Lucas, 2008) and the upper part of eolian Navajo Sandstone (Blakey et al., 1988) could represent the coeval strata with sediments of similar climate in the Colorado Plateau. It might be an interruption of relatively cool ($\sim$ 9 to 18 °C) continental climate inferred from oxygen and hydrogen isotope composition of chert precipitated in inter-dune, freshwater lakes in the Navajo Sandstone (Kenny, 2015). In eastern England, the co-occurrence of the acmes of thermophilic pollens *Classopollis classoides* and *Liasidium variabile* indicates a warm and humid climate in the late Sinemurian (Riding et al., 2013), likely illustrating a different climate scenario in Europe.

5.1.3 The Pliensbachian age

The Ma'anshan Member of the Pliensbachian displays a prominent change in the distribution and extent of red color sediment and pedogenesis. The reddish sediments extend through the entire member (cf. Figs. 6 and S2) and can be ob-

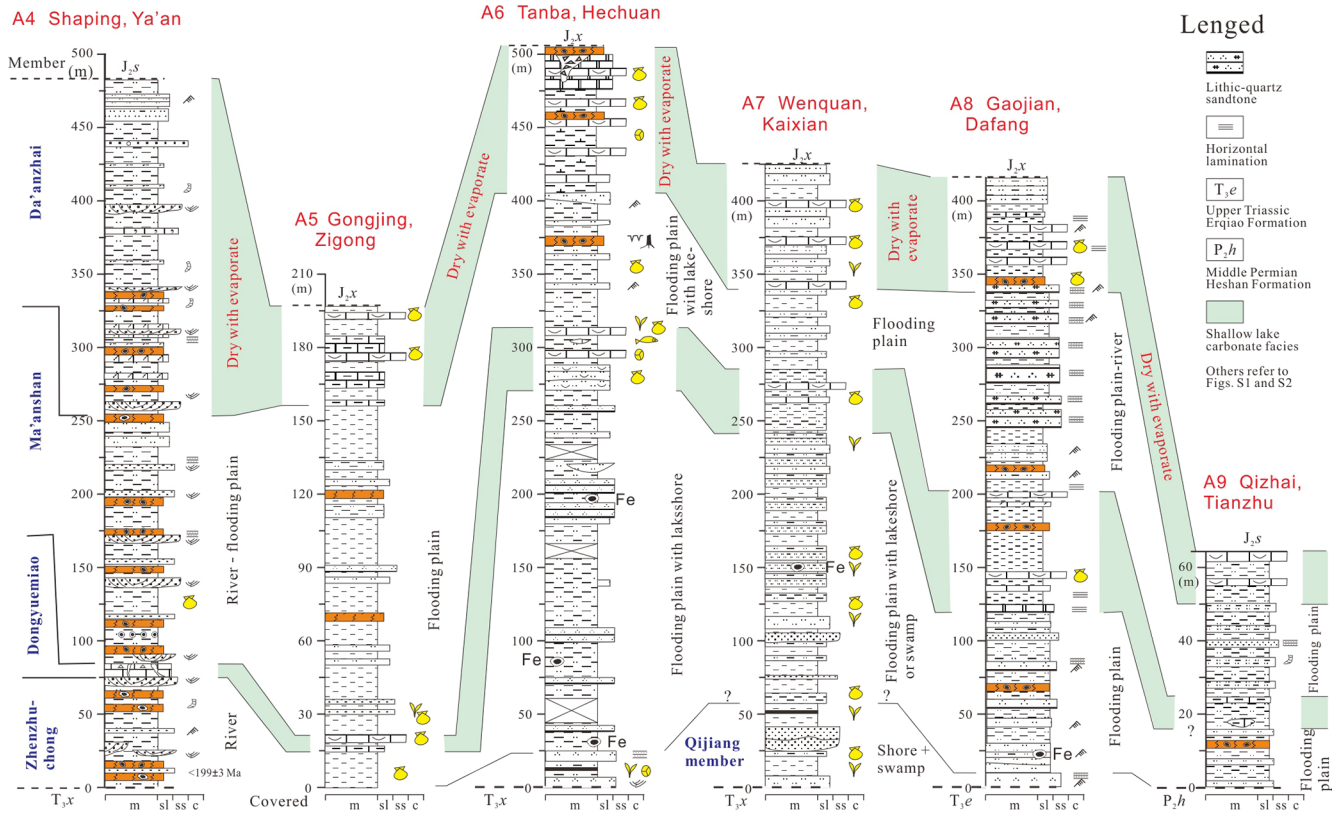

Figure 7. Stratigraphic correlation and depositional environment interpretation of the Lower Jurassic in the GSB. Data of each section refer to Fig. 1. Note, two lacustrine transgressive cycles are marked by correlative pale green areas.

served across most of the GSB. Calcisols are documented in both the western and central GSB (Figs. 6, 7, S1, and S2). A total of 10 calcisol horizons were recognized at the Shaping section, Ya'an (Figs. 6 and S1). Strongly leached pedogenic structures and mudcracks are seen in Bed H8 of the Tanba section, Hechuan (Fig. 3a and d). Abundant calcretes within terrestrial red mudrocks are widely described at Gaoxian of Dafang (Location A8; Zhang et al., 2016), Hulukou of Weiyuan (Location A10; SBG, 1980), Geyaoguan of Gulin (Location A13; SBG, 1976), Taiyuan of Fengdu (Location A16; SBG, 1975), and Yaxi of Zunyi (Location A17; Yang, 2015). The widespread distribution of redbeds and calcisols (Figs. 4 and 7) denotes an intensification of the (semi)arid climate.

Plant and sporopollen fossils also show a change to drier climate in the Pliensbachian. Compared to the Sinemurian members, more plant fossils are reported in this member (e.g., Meng and Chen, 1997; Wang et al., 2010). The Pliensbachian–Toarcian sporopollen assemblages are dominated by a sporomorph genera assemblage of *Dictyophyllidites*, *Cyathidites*, and *Classopollis*, in which the dry-type gymnosperm spore *Classopollis* is more prevalent than in the Hettangian–Sinemurian (Zhang and Meng, 1987).

A similar dry temperate or subtropical climate is interpreted for the upland coniferous forest in Qaidam Basin in northwestern China (Wang et al., 2005) and by inter-dune playa mudstones of the Kayenta Fm in the Colorado Plateau (e.g., Bromley, 1992), although there was a cool and humid climate in southern Kazakhstan, central Asia (Tramoy et al., 2016).

5.1.4 The Toarcian age

In spite the fact that the Da'anzhai Member was deposited in the largest lacustrine transgression period (Fig. 7; for details see Supplement Note S1), abundant evidence for arid conditions, including backshore reddish mudrocks with calcisols, lacustrine micritic dolomites and/or gypsum, and stable isotopic geochemistry of lacustrine carbonate, indicate that the Toarcian aridification could be the most intensive of the late Early Jurassic in the GSB.

Redbeds with abundant calcretes are well developed in this member (Figs. 4 and 7). Four calcisols in the Shaping section (Figs. 6 and S1) and the leaching/illuvial structure (Bed H13) in the Tanba section (Fig. 3c) were observed. Calcisols with calcretes also occur at sections of Dafang (Location A8; Zhang et al., 2016), Nanxi (Location A11; SBG 1980), Gongxian (Location A12; Liang et al., 2006), and Yunyang (Location A15; Meng et al., 2005). The widespread occurrence of calcisols within the lacustrine facies reveals that sub-

aerial exposure of sediments often interrupted the lake environment, illustrating dynamic lake-level fluctuations and an arid climate.

Gypsum and micritic dolomites are reported in the western and southern GSB (SBG, 1980; Mo and Yu, 1987; Peng, 2009; and this work) (Figs. 1, 4, and 7). Though there are a number of hypotheses on the dolomite formation in deep time, such as authigenic origin, diagenetic replacement, microbial mediation (e.g., Vasconcelos et al., 1995; Mckenzie and Asconcelos, 2009; Petrash et al., 2017), a high abundance of dolomite was interpreted as forming during greenhouse periods, characterized by warm climates, probably reflecting favorable conditions for evaporite deposition and dolomitization via hypersaline reflux (Warren, 2000). Dolomites are also thought to be the result of interplay of climate with sea level and base level change (e.g., Newport et al., 2017) or of interaction with climatic regimes (Vandeginste et al., 2012). The widespread micritic dolomites in the Da'anzhai Member, which are associated with gypsum (Fig. 3f), likely indicate an arid climate in the central and western GSB (Fig. 1b). Gypsum occasionally occurs at Maliuping of Hechuan (Fig. 3f) and Wujiaba of Zigong (SBG, 1980), showing a possible evaporitic climate in the early Toarcian in the central GSB.

Carbon and oxygen isotopes of lacustrine carbonates further support the interpretation of an arid climate in the Toarcian age in the GSB. The mainly positive $\delta^{13}C$ values, 0 to 2 ‰ (Fig. 5), from Hechuan (Wang et al., 2006) indicate the lakes were brackish or even saline. The relatively heavy negative $\delta^{13}C$ values, -1 ‰ to -3.5 ‰ (Fig. 5), from Zigong (Wang et al., 2006) and Ya'an (this work) denote low depletions of ^{13}C during calcite and aragonite precipitation and mean that the lakes were possibly brackish. Lightly negative $\delta^{18}O$ values, -5 ‰ to -12 ‰ (Fig. 5), of the lacustrine carbonates suggest closed lacustrine, palustrine, and pond systems formed in a regional arid or semiarid climate with evaporation exceeding precipitation.

The covariance of $\delta^{13}C$ and $\delta^{18}O$ is a criterion to distinguish closed or open lakes (e.g., Talbot, 1990; Li and Ku, 1997). Pronounced positive covariances ($R^2 = 0.44$–0.96) between carbon and oxygen isotopes (Fig. 5) indicate a typical arid–semiarid pattern of lakes in the central and western GSB.

The Da'anzhai Member has the same palynofloral assemblage with the Ma'anshan Member, in which the dry-type gymnosperm spore *Classopollis* is more abundant than in underlying strata (e.g., Zhang and Meng, 1987; Wang et al., 2010), supporting the aridification indicated by climate-sensitive sediments and stable isotope ratios of lacustrine carbonates mentioned above.

Coastal Cheirolepidiacean (gymnosperm) forests indicate (temperate to subtropical) warm and humid climate punctuated by locally dry and/or arid events in the Toarcian in Qaidam Basin in northwestern China (Wang et al., 2005). In Inner Mongolia in northern China, thermophilous plants, such as the dipteridaceous fern *Hausmannia*, Bennettitales *Ptilophyllum*, display similar warm and humid climate interrupted by hot and even arid conditions in a short intervals of the Toarcian (Deng et al., 2017). The warm and wet climate was also indicated by assemblages of sporomorph and vegetation in the late Early Jurassic in Jurong of Jiangsu, in the Lower Yangtze area (Huang et al., 2000). In southern Kazakhstan, central Asia, paleoflora and δ^2H values suggest slightly less humid and warmer conditions starting from the early Toarcian (Tramoy et al., 2016).

Climate-sensitive sediments, carbon and oxygen isotope values and covariance, and palynoflora together indicate that an overall (semi)arid climate dominated the GSB during the Early Jurassic, possibly accompanied by occasional evaporitic climate. Relatively abundant calcisols suggest that the GSB was in a subtropical arid zone based on the paleoclimatic zonation model of paleosols (Mack and James, 1994) during the middle-late Early Jurassic. Through the Early Jurassic, this (semi)arid climate in GSB is thoroughly comparable with the simultaneous arid climate recorded in dryland lacustrine and eolian facies in the Colorado Plateau (e.g., Blakey et al., 1988; Bromley, 1992; Tanner and Lucas, 2008; Parrish et al., 2017) but distinct from the relatively warm and humid climate indicated by sedimentological and floral characteristics in northern China (e.g., Wang et al., 2005; Deng et al., 2017) and in relatively high latitudes of the Southern Hemisphere (Pole, 2009).

In summary, the increasing aridity and warming in the GSB and arid climate in the Colorado Plateau could have been consecutive through the Early Jurassic and seems to not be harmonized with the global fluctuated climate that could be imprinted by two large volcanic eruptions of the Central Atlantic magmatic province and Karro–Ferrar large igneous province. The secular arid climate in the two areas is more probably constrained by paleotopography, where both were laid in the relatively low latitudes 15–30° N (Fig. 1a).

5.2 pCO_2 perturbations and events

Pedogenic carbonates found in various continental settings precipitate in direct contact with soil atmosphere and bedrock and hold a meaningful signature of past climate (Alonso-Zarza and Tanner, 2006). There are few high age resolution pCO_2 reconstructions for the Early Jurassic. The pCO_2 estimates have a focus on the event horizons, such as the transition from the Triassic to Jurassic (e.g., Tanner et al., 2001; Schaller et al., 2011). Herein we present a pCO_2 estimate based on data from the GSB at ~ 1.0 Myr age resolution for a ~ 20 Myr (199–179 Ma) interval of the Early Jurassic (Figs. 6 and 8a).

5.2.1 pCO_2 perturbation

Results of model estimates show that the pCO_2 values range from 980 to 2610 ppmv with a mean 1660 ppmv in

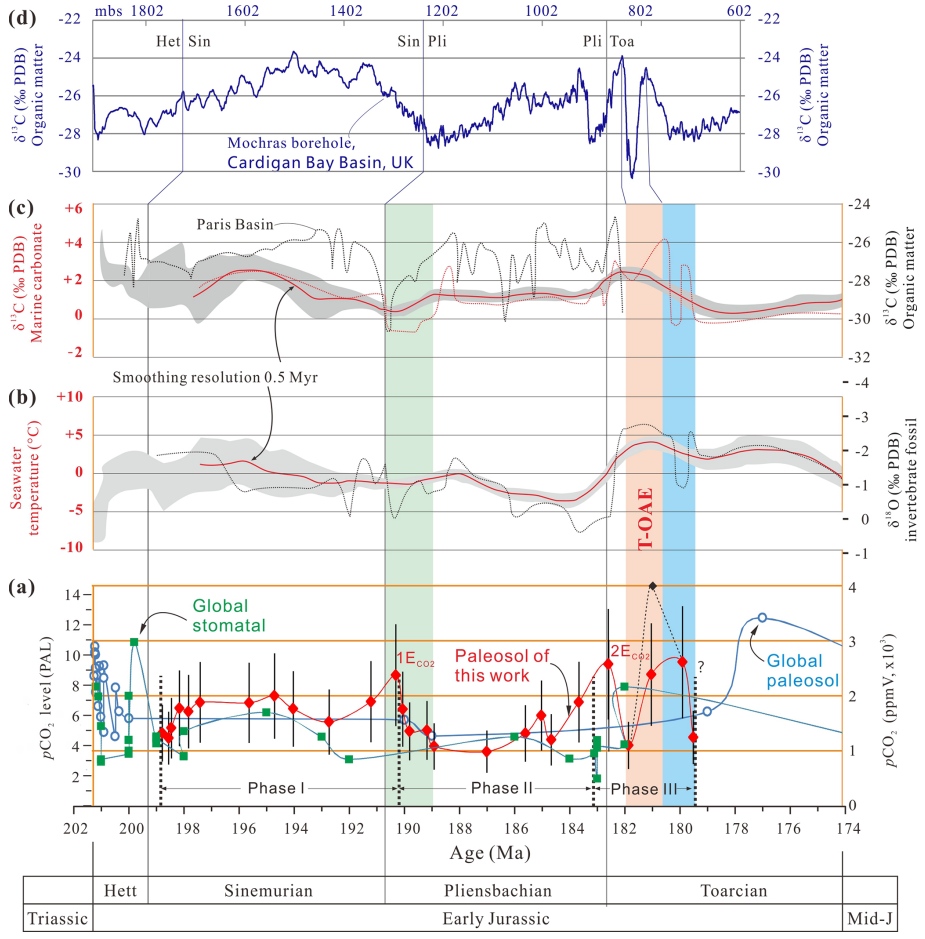

Figure 8. Comparison among the Early Jurassic pCO_2, $\delta^{13}C$ of marine carbonates and organic matter, $\delta^{18}O$ of invertebrate fossils, and seawater temperature. Age model is from Cohen et al. (2013). **(a)** The pCO_2 values of this work and the composite pCO_2 by paleosol and stomatal index (Supplement Tables S6 and S7). Vertical bars are errors (1σ) of pCO_2 (Table S5). Errors are propagated using the Gaussian approach (Breecker and Retallack, 2014). Note that (1) $pCO_2 = 4027$ ppmv (black solid diamond, sample J1z-20-01) if the $\delta^{13}C_r = -29.0‰$ at 181 Ma, taken from Xu et al. (2018), in the case of other constant parameters. (2) The early published pCO_2 values from both carbon isotope of pedogenic carbonates and stomatal index of fossil plants (data refer to Tables S6 and S7) were very roughly dated using the average age of a lithostratigraphic formation or group, with which the uncertainty can be up to 10 Myr, leading to the difficulty of precise and accurate pCO_2 correlation in pace, frequency, and event. **(b)** The $\delta^{18}O$ and seawater temperature (dotted black line) of marine invertebrate fossils compiled from Rosales et al. (2001), Jenkyns et al. (2002), Bailey et al. (2003), van de Schootbrugge et al. (2005), Gómez et al. (2008), Metodiev and Koleva-Rekalova (2008), Suan et al. (2008), Korte et al. (2009), Dera et al. (2011), and Gómez et al. (2016). **(c)** The dotted red line shows $\delta^{13}C$ of marine carbonates in the western Tethys Ocean, composed from Jenkyns and Clayton (1986, 1997), Hesselbo et al. (2000), Dera et al. (2011), Arabas et al., 2017; the dotted and solid black line $\delta^{13}C$ of organic matters from Paris Basin, France (Peti et al., 2017). Smoothed $\delta^{18}O$ and seawater temperature (red curves) in **(b)** and **(c)** are following Dera et al. (2011). **(d)** The $\delta^{13}C$ of organic matter from the North Atlantic taken from the Mochras borehole, Cardigan Bay Basin, UK (Xu et al., 2018; Storm et al., 2020), with a seven-point average smoothing against depth (mbs).

the Early Jurassic after the Hettangian and can be divided into three intervals (Figs. 6 and 8a): phase I, stable 1500–2000 ppmv (mean ~1700 ppmv) in the Zhenzhuchong and Dongyuemiao members (Sinemurian age); phase II, main 1000–1500 ppmv (mean ~1300 ppmv) in the Ma'anshan Member (Pliensbachian age); and phase III, great fluctuation 1094–2610 ppmv (mean ~1980 ppmv) in the lower Da'anzhai Member (early Toarcian age).

The evolution and level of pCO_2 estimated by carbon isotope ratios of the pedogenic carbonates from the GSB compare favorably with the global composite based on the plant stomata method (for data of the composite curve, see Table S6) but show significant differences relative to the global composite pCO_2 based on paleosols (Fig. 8a; Suchechi et al., 1988; Cerling, 1991; Ekart et al., 1999), which may be attributed to the shortage (<4 samples) of global data and large age uncertainties (Fig. 8a and Tables S5 and S6).

The changes in pCO_2 from the GSB have a similar pattern to coeval seawater temperature estimates through the Early Jurassic, although there are some discrepancies in pace and in detail (cf. Fig. 8a and b). Therefore, the relatively high pCO_2 1500–2000 ppmv approximately corresponds to the relatively high seawater mean temperature −2 to +2 °C in the Sinemurian, low pCO_2 1000–1500 ppmv corresponds to low seawater mean temperature −5 to −2 °C in the Pliensbachian, and quick rising pCO_2 of 1200 ppmv to ∼ 2500 ppmv corresponds to the rapidly increased seawater temperature of −4 to +4 °C in the late Pliensbachian–early Toarcian.

The pCO_2 record roughly trends with the carbon isotope records of marine carbonates and organic matter (cf. Fig. 8a to c and d), suggesting a possible linkage of the pCO_2 record in the GSB to the global carbon cycle (see Sect. 5.2.2). Nevertheless, it is difficult for the proxies to compare in a higher detail, making it difficult to relate the record to orbital forcing of the global carbon cycle in the Sinemurian–Pliensbachian (Storm et al., 2020).

As a greenhouse gas, atmospheric CO_2 has a strong control over global temperatures for much of the Phanerozoic (e.g., Crowley and Berner, 2001; Royer, 2006; Price et al., 2013), but a decoupling of CO_2 and temperature has also been suggested (e.g., Veizer et al., 2000; Dera et al., 2011; Schaller et al., 2011). The pattern of the Early Jurassic pCO_2 reconstructed from the carbon isotope of pedogenic carbonates in the GSB in southwestern China supports the coupled relationship of CO_2 with temperature. Models of the coupling and decoupling of CO_2–temperature and the CO_2–carbon cycle have to consider (1) the age order of CO_2–temperature and carbon cycle relevance, i.e. they should be related in the same age (long-term or short-term) hierarchy; (2) precise age constraints of individual CO_2 and temperature data; (3) methods of CO_2 and temperature estimates, depending on precondition, presumptions, parameters, uncertainty, sample diagenesis, etc.; and (4) controls or influences of key factors such ice sheets, tectonics, paleogeography, cosmic ray fluxes, biota, volcanic eruptions, and so on.

5.2.2 Rapid pCO_2 falling events

The GSB Early Jurassic pCO_2 curve reveals two rapid falling events (Figs. 6 and 8a). The first event ($1E_{CO_2}$) shows a quick drop from ∼ 2370 ppmv (sample J1z-08-01 at depth 84.7 m) to 1350 ppmv (sample J1z-10-02 at depth 94.4 m), near the boundary of the Dongyuemiao and Ma'anshan Members (Fig. 6), or to 1075 ppmv (sample J1z-11-02 at depth 111.7 m), which took place in the early Pliensbachian (∼ 190.4–189.9/189.1 Ma; Fig. 8c). The extent of the rapidly falling pCO_2 is ∼ 1000–1300 ppmv in 9.7–17.0 m. In other words, a ∼ 1000 ppmv drop could be accomplished within ∼ 0.5–1.0 Myr based on the estimate of sedimentation rate (Table S4).

While the corresponding early Pliensbachian climatic and isotopic-shifting events are not observed in the smoothed curves of the Early Jurassic seawater temperature and carbon cycle (Dera et al., 2011), the rapid-falling event $1E_{CO_2}$ is well correlated to the nearly coeval excursion events of carbon and oxygen isotopes recorded in western Tethys and the North Atlantic (Fig. 8). The $1E_{CO_2}$ event compares well to (1) the rapid carbon isotope negative excursion of (oysters, belemnites, and brachiopods) shells from the Cleveland Basin, UK (Korte and Hesselbo, 2011), and northwest Algeria (Baghli et al., 2020); (2) that of organic matter and marine carbonates from southern Pairs Basin (Bougeault et al., 2017; Peti et al., 2017) and Cardigan Bay Basin, UK (Storm et al., 2020); and (3) rapid oxygen isotope negative excursion (seawater warming) of belemnites from northern Spain (van de Schootbrugge et al., 2005). The rapid change of the stable isotope record has been called the Sinemurian–Pliensbachian boundary event (SPBE) and dated in the ammonite of the upper *raricostatum* and lower *jamesoni* zones (Bougeault et al., 2017).

The second event $2E_{CO_2}$ displays a large drop of 2574 ppmv (sample J1z-18-01 at depth 252.7 m) to 1094 ppmv (sample J1z-19-01 at depth 272.3 m), a ∼ 1500 ppmv decrease within 19.6 m (estimated age interval ∼ 0.8 Myr; Table S4 and Fig. 8a). Following the second drop, pCO_2 rises rapidly by ∼ 1300 ppmv from 1094 to 2386 ppmv (sample J1z-20-01 at depth 294.3 m), although only a few samples support the this cycle of pCO_2 falling–rising.

Strata in western Sichuan (Xu et al., 2017) may correlate to the time interval of the T-OAE, during which pCO_2 doubled over background values, from ∼ 1000 ppmv to ∼ 2000 ppmv (e.g., Beerling and Royer, 2002; McElwain et al., 2005; Berner, 2006). Given that chronostratigraphic correlation is challenging, the pCO_2 falling–rising cycle might correspond to the quickly shifting cycle of stable isotopes during the T-OAE (Fig. 8a, c–d). In detail, the rapid falling–rising of pCO_2 is consistent with (1) the quick negative–positive carbon isotope excursion of marine carbonates from Italy (Jenkyns and Clayton, 1986; Sabatino et al., 2009), England and Wales (Jenkyns and Clayton, 1997), northern Spain (van de Schootbrugge et al., 2005), the Lusitanian Basin of Portugal (Hesselbo et al., 2007), the Paris Basin (Hermoso et al., 2009), and Morocco (Bodin et al., 2016); (2) the invertebrate calcareous shells from the Cleveland Basin in the UK (Korte and Hesselbo, 2011) and northwestern Algeria (Baghli et al., 2020); (3) the marine organic matter from Morocco (Bodin et al., 2016), Yorkshire (Cohen et al., 2004; Kemp et al., 2005) and the Cardigan Bay Basin in the UK (Xu et al., 2018), northern Germany (van de Schootbrugge et al., 2013), Alberta and British Columbia in Canada (Them II et al., 2017), northern Tibet (Fu et al., 2016), and Japan (Izumi et al., 2018); (4) the terrestrial organic matter from the Sichuan Basin in China (Xu et al., 2017); and (5) the quick oxygen isotope negative–positive shifting (seawater warming) of bra-

chiopods (Suan et al., 2008) and fossilized wood (Hesselbo et al., 2007) from the Lusitanian Basin in Portugal.

Multiple hypotheses have been proposed to interpret the 5–6 °C decrease of sea surface temperatures in the late Pliensbachian (Bailey et al., 2003; van de Schootbrugge et al., 2005; Suan et al., 2010) and warming of ∼ 8 °C in the early Toarcian (Bailey et al., 2003; Suan et al., 2010), such as the sea level falling and rising, methane release, a Karoo–Ferrar eruption, the Hispanic corridor opening, etc. Perhaps these hypotheses somewhat explain the rapid change of sea surface temperatures but might not link to drastic falling of pCO_2. As we know, atmospheric CO_2 is controlled by volcanism, weathering, vegetation on land and phytoplankton in the ocean, and orbital forcing. The Sr isotope curve shows a rapid change in the early Toarcian but does not show a change in the early Pliensachian (e.g., Jones et al., 1994), indicating a distinct transfer of weathering took place on the land only at the time of the T-OAE. No robust evidence shows the rapid changes of terrestrial vegetation and marine primary productivity for the two intervals, except for the floral change in western Tethys during the T-OAE (Slater et al., 2019). The Karoo–Ferrar eruption could be responsible for the rapid rising of pCO_2 but not for the falling. The orbital forcing might be an alternative for explaining this.

To sum up, the rapid falling events of the Early Jurassic pCO_2 values in the GSB are compatible with the response of stable isotopes (carbon cycle) and seawater temperature from coeval marine sediments in a total tendency and eventful change but are not harmonized at a high-resolution timescale. Whatever caused the rapid variations of sea surface temperatures, stable isotopes, and pCO_2, their near concordance suggests that it is a positive feedback of the sea surface temperature and carbon cycle to the pCO_2 in trend and event through the Early Jurassic, whereas the higher frequency changes in the Sinemurian–Pliensbachian may support other causal driving of the climate, such as orbital forcing (Storm et al., 2020).

6 Conclusions

Based on analyses of climate-sensitive sediments and stable isotopes and the reconstruction of paleoclimate and pCO_2, we make the following conclusions.

1. An overall warm and hot and (semi)arid climate dominated the GSB during the Early Jurassic, possibly accompanied by an occasionally evaporitic climate in the Toarcian. This (semi)arid climate in GSB is comparable with that in the Colorado Plateau, western North America, but distinct from the relatively warm and humid terrestrial climate recognized in other places on the Chinese mainland (e.g., Qaidam, Inner Mongolia, and the Lower Yangtze) and the high latitudes of the Southern Hemisphere.

2. The Early Jurassic pCO_2 values show that a range between 980 and 2610 ppmv is ∼ 3.5–10 times the pre-industrial value 275 ppmv and that the mean 1720 ppmv is ∼ 6 times the pre-industrial value. Three phases of pCO_2 values were distinguished: 1500–2000 ppmv (mean ∼ 1700 ppmv) in the Sinemurian age, 1000–1500 ppmv (mean ∼ 1300 ppmv) in the Pliensbachian age, and 1094–2610 ppmv (mean ∼ 1980 ppmv) in the early Toarcian. Two events of rapidly falling pCO_2 were also recognized: a ∼ 1000–1300 ppmv drop at the Sinemurian–Pliensbachian boundary and a quickly falling (rising) event of ∼ 1500 ppmv in the early Toarcian. The phases and events manifest the perturbation of pCO_2 in the Early Jurassic.

3. The perturbation and rapid falling events of the Early Jurassic pCO_2 from the GSB are compatible with the carbon cycle and seawater temperature from coeval marine sediments in the North Atlantic and western Tethys in terms of total tendency and eventful change. The compatibility suggests that there is a positive linkage of the sea surface temperature and carbon cycle to the pCO_2 through the Early Jurassic. On the contrary, differences at a high-resolution timescale imply additional climate drivers, such as orbital forcing, are important in the Sinemurian–Pliensbachian record.

Data availability. All the data are available in the Supplement.

Supplement. The supplement related to this article is available online at: https://doi.org/10.5194/cp-16-2055-2020-supplement.

Author contributions. XL designed the concept and working idea and created the paper text, tables, and figures. JW took part in the field work and contributed to writing the paper and analyzing carbon and oxygen isotopes. TR polished the language and advised on some ideas. MZ, ZW, and CZ took part in field work and took some samples.

Competing interests. The authors declare that they have no conflict of interest.

Acknowledgements. We thank Helmut Weissert and Dan Breecker for careful scrutiny and constructive comments and suggestions.

Financial support. This research has been supported by the National Natural Science Foundation of China (grant no. 41672097).

Review statement. This paper was edited by Appy Sluijs and reviewed by Dan Breecker and Helmut Weissert.

References

Alonso-Zarza, A. M. and Tanner, L. H.: Preface, in: Paleoenvironmental Record and Applications of Calcretes and Palustrine Carbonates, Geol. Soc. Am. Spec. Pap., 416, V–VII, https://doi.org/10.1130/0-8137-2416-3.v, 2006.

Arabas, A., Schlogl, J., and Meiste C.: Early Jurassic carbon and oxygen isotope records and seawater temperature variations: Insights from marine carbonate and belemnite rostra (Pieniny Klippen Belt, Carpathians), Palaeogeogr. Palaeocl., 485, 119–135, 2017.

Arens, N. C., Jahren, A. H., and Amundson, R.: Can C3 plants faithfully record the carbon isotopic composition of atmospheric carbon dioxide, Paleobiology, 26, 137–164, 2000.

Arias, C.: Extinction pattern of marine Ostracoda across the Pliensbachian-Toarcian boundary in the Cordillera Ibérica, NE Spain: Causes and consequences, Geobios, 42, 1–15, 2009.

Baghli, H., Mattioli, E., Spangenberg, J. E., Bensalah, M., Arnaud-Godet, F., Pittet, B., and Suan, G.: Early Jurassic climatic trends in the south-Tethyan margin, Gondwana. Res., 77, 67–81, https://doi.org/10.1016/j.gr.2019.06.016, 2020.

Bailey, T. R., Rosenthal, Y., McArthur, J. M., van de Schootbrugge, B., and Thirlwall, M. F.: Paleoceanographic changes of the Late Pliensbachian-Early Toarcian interval: a possible link to the genesis of an Oceanic Anoxic Event, Earth Planet. Sci. Lett., 212, 307–320, 2003.

Beerling, D. J. and Royer, D. L.: Reading a CO_2 signal from fossil stomata, New Phytol., 153, 387–397, https://doi.org/10.1046/j.0028-646X.2001.00335.x, 2002.

Berner, R. A.: GEOCARBSULF: A combined model for Phanerozoic atmospheric O_2 and CO_2, Geochim. Cosmochim. Ac., 70, 5653–5664, 2006.

Besse, J. and Courtillot, V.: Paleogeographic maps of the continents bordering the Indian Ocean since the Early Jurassic, J. Geophys. Res., 93, 11791–11808, 1988.

Blakey, R. C., Peterson, F., and Kocurek, G.: Synthesis of late Paleozoic and Mesozoic eolian deposits of the Western Interior of the United States, Sediment. Geol., 56, 3–125, https://doi.org/10.1016/0037-0738(88)90050-4, 1988.

Bodin, S., Krencker, F. N., Kothe, T., Hoffmann, R., Mattioli, E., Heimhofer, U., and Kabiri, L.: Perturbation of the carbon cycle during the late Pliensbachian – early Toarcian: New insight from high-resolution carbon isotope records in Morocco, J Afri. Earth Sci., 116, 89–104, https://doi.org/10.1016/j.jafrearsci.2015.12.018, 2016.

Boucot, A. J., Chen, X., Scotese, C. R., and Morley, R. J.: Phanerozoic Paleoclimate: An Atlas of Lithologic Indicators of Climate, SEPM Concepts in Sedimentology and Paleontology, SEPM, Tulsa, 11, 1–478, 2013.

Bougeault, C., Pellenard, P., Deconninck, J. F., Hesselbo, S. P., Dommergues, J. L., Bruenau, L., Cocquerez, T., Laffont, R., Huret, E., and Thibault, N.: Climatic and palaeoceanographic changes during the Pliensbachian (Early Jurassic) inferred from clay mineralogy and stable isotope (C–O) geochemistry (NW Europe), Global Planet. Change, 149, 139–152, 2017.

Breecker, D. O.: Quantifying and understanding the uncertainty of atmospheric CO_2 concentrations determined from calcic paleosols, Geochem. Geophys. Geosyst., 14, 3210–3220, 2013.

Breecker, D. O. and Retallack, G. J.: Refining the pedogenic carbonate atmospheric CO_2 proxy and application to Miocene CO_2, Palaeogeogr. Palaeocl., 406, 1–8, 2014.

Breecker, D. O., Sharp, Z. D., and McFadden, L. D.: Atmospheric CO_2 concentrations during ancient greenhouse climates were similar to those predicted for A.D. 2100, P. Natl. Acad. Sci. USA, 107, 576–580, 2009.

Breecker, D. O., Sharp, Z. D., and McFadden, L. D.: Seasonal bias in the formation and stable isotope composition of pedogenic carbonate in modern soil from central New Mexico, USA, Geol. Soc. Am. Bull., 12, 630–640, 2010.

Bromley, M.: Topographic inversion of early interdune deposits, Navajo Sandstone (Lower Jurassic), Colorado Plateau, USA, Sediment. Geol., 80, 1–25, 1992.

Buchmann, N., Brooks, R. J., Flanagan, L. B., and Ehleringer, J. R.: Carbon isotope discrimination of terrestrial ecosystems, in: Stable Isotopes: Integration of Biological, Ecological and Geochemical Processes, edited by: Griffiths, H., BIOS Scientific Publications, Oxford, UK, 203–221, 1998.

Caruthers, A. H., Smith, P. L., and Gröcke, D. R.: The Pliensbachian-Toarcian (Early Jurassic) extinction, a global multi-phased event, Palaeogeogr. Palaeocl., 386, 104–118, 2013.

Cerling, T. E.: Carbon dioxide in the atmosphere: evidence from Cenozoic and Mesozoic paleosols, Am. J. Sci., 291, 377–400, 1991.

Cerling, T. E.: Stable carbon isotopes in palaeosol carbonates, in: Palaeoweathering, palaeosurfaces and related continental deposits, edited by: Thiry, M. and Simm-CoinÇon, R., Spec. P. Intl. Asso. Sedi., 27, 43–60, 1999.

Cleveland, D. M., Nordt, L. C., Dworkin, S. I., and Atchley, S. C.: Pedogenic carbonate isotopes as evidence for extreme climatic events preceding the Triassic-Jurassic boundary: implications for the biotic crisis?, Geol. Soc. Am. Bull., 120, 1408–1415, 2008.

Cohen, A. S., Coe, A. L., Harding, S. M., and Schwark, L.: Osmium isotope evidence for the regulation of atmospheric CO_2 by continental weathering, Geology, 32, 157–160, 2004.

Cohen, K. M., Finney, S. C., Gibbard, P. L., and Fan, J. X.: The ICS International Chronostratigraphic Chart, Episodes, 36, 199–204, 2013 (updated 2013).

Crowley, T. J. and Berner, R. A.: CO_2 and climate change, Science, 292, 870–872, 2001.

Deng, S. H., Zhao, Y., Lu, Y. Z., Shang, P., Fan, R., Li, X., Dong, S. X., and Liu, L.: Plant fossils from the Lower Jurassic coal-bearing formation of central InnerMongolia of China and their implications for palaeoclimate, Palaeoworld, 26, 279–316, 2017.

Dera, G., Pellenard, P., Neige, P., Deconinck, J. F., Pucéat, E., and Dommergues, J. L.: Distribution of clay minerals in Early Jurassic Peritethyan seas: Palaeoclimatic significance inferred from multiproxy comparisons, Palaeogeogr. Palaeocl., 271, 39–51, https://doi.org/10.1016/j.palaeo.2008.09.010, 2009.

Dera, G., Brigaud, B., Monna, F., Laffont, R., Pucéat, E., Deconinck, J. F., Pellenard P., Joachimski, M. M., and Durlet, C.: Climatic ups and downs in a disturbed Jurassic world, Geology, 39, 215–218, 2011.

Dong, Z. M.: A new prosauropod from Ziliujing Formation of Sichuan Basin, Vertebrat. Palasiatic., 22, 310–313, 1984 (in Chinese with English abstract).

Duan, S. Y. and Chen, Y.: Mesozoic fossil plants and coal formation of eastern Sichuan Basin, in: Continental Mesozoic Stratigraphy and Paleontology in Sichuan Basin of China: Part II, Paleontological Professional Papers, People's Publ. House Sichuan, Chengdu, 491–519, 1982 (in Chinese).

Ekart, D. D., Cerling, T. E., Montñez, I. P., and Tabor, N. J.: A 400 million year carbon isotope record of pedogenic carbonate: implications for paleoatmospheric carbon dioxide, Am. J. Sci., 299, 805–827, 1999.

Flügel, E.: Microfacies of Carbonate Rocks: Analysis, Interpretation and Application, Springer-Verlag, Berlin, 976 pp., 2004.

Friedli, H., Lotscher, H., Oeschger, H., Siegenthale, U., and Stauffer, B.: Ice core record of the $^{13}C/^{12}C$ ratio of atmospheric CO_2 in the past two centuries, Nature, 324, 237–238, 1986.

Fu, X. G., Wang, J., Feng, X. L., Wang, D., Chen, W. B., Song, C. Y., and Zeng, S. Q.: Early Jurassic carbon-isotope excursion in the Qiangtang Basin (Tibet), the eastern Tethys: implications for the Toarcian Oceanic anoxic event, Chem. Geol., 442, 67–72, 2016.

Gómez, J. J. and Goy, A.: Warming-driven mass extinction in the Early Toarcian (Early Jurassic) of northern Spain, Correlation with other time-equivalent European sections, Palaeogeogr. Palaeocl., 306, 176–195, 2011.

Gómez, J. J., Goy, A., and Canales, M. L.: Seawater temperature and carbon isotope variations 15 in belemnites linked to mass extinction during the Toarcian (Early Jurassic) in Central and Northern Spain. Comparison with other European sections, Palaeogeogr. Palaeocl., 258, 28–58, 2008.

Gómez, J. J., Comas-Rengifo, M. J., and Goy, A.: Palaeoclimatic oscillations in the Pliensbachian (Early Jurassic) of the Asturian Basin (Northern Spain), Clim. Past, 12, 1199–1214, https://doi.org/10.5194/cp-12-1199-2016, 2016.

Guo, L. Y., Zhang, S. W., Xie, X. N., Li, Z. S., Huang, C. Y., and Chen, B. C.: Geochemical characteristics and organic matter enrichment of the Dongyuemiao Member mudstone of Lower Jurassic in the Western Hubei-Eastern Chongqing, Earth Sci., 42, 1235–1246, 2017 (in Chinese with English abstract).

Guo, Z. W, Deng, K. L., and Han, Y. H.: Formation and Evolution of the Sichuan Basin, Geo. Publ. House, Beijing, 200 pp., 1996.

Hallam, A. and Wignall, P. B.: Mass extinctions and sea-level changes, Earth Sci. Rev., 48, 217–250, 1999.

He, T. H. and Liao, C. F.: Control of Upper Triassic division and correlation and Indosinian Movement on oil and gas accumulation in Sichuan Basin, Acta Geol. Sichuan, 00, 40–55, 1985 (in Chinese).

Hermoso, M., Le Callonnec, L., Minoletti, F., Renard, M., and Hesselbo, S. P.: Expression of the Early Toarcian negative carbon-isotope excursion in separated carbonate microfractions (Jurassic, Paris Basin), Earth Planet. Sci. Lett., 277, 194–203, 2009.

Hesselbo, S. P. and Jenkyns, H. C.: British Lower Jurassic sequence stratigraphy, in: Mesozoic-Cenozoic Sequence Stratigraphy of European Basins, edited by: de Graciansky, P. C., Hardenbol, J., Jacquin, Th., and Vail, P. R., SEPM Spec. P., 60, 562–581, 1998.

Hesselbo, S. P., Gröcke, D. R., Jenkyns, H. C., Bjerrum, C. J., Farrimond, P., Morgans Bell, H. S., and Green, O. R.: Massive dissociation of gas hydrate during a Jurassic oceanic anoxic event, Nature, 406, 392–395, https://doi.org/10.1038/35019044, 2000.

Hesselbo, S. P., Jenkyns, H. C., Duarte, L. V., and Oliveira, L. C. V.: Carbon-isotope record of the Early Jurassic (Toarcian) Oceanic Anoxic Event from fossil wood and marine carbonate Lusitanian Basin, Portugal, Earth Planet. Sci. Lett., 253, 455–470, 2007.

Huang, C. J. and Hesselbo, S. P.: Pacing of the Toarcian Oceanic Anoxic Event (Early Jurassic) from astronomical correlation of marine sections, Gondwana Res., 25, 1348–1356, https://doi.org/10.1016/j.gr.2013.06.023, 2014.

Huang, P., Guan, Y. M., and Yang, X. Q.: Early Jurassic palynoflora from a drilling section of Jurong, Jiangsu, Acta Micropalaeontol. Sin., 17, 85–98, 2000.

Huang, Q. S.: Paleoclimate and coal-forming characteristics of the Late Triassic Xujiahe stage in northern Sichuan, Geol. Rev., 41, 92–99, 1995 (in Chinese with English abstract).

Huang, Q. S.: The flora and paleoenvironment of the Early Jurassic Zhenzhuchong Formation in Daxian-Kaixian region, northern margin of the Sichuan Basin, Ear. Sci. J. China Uni. Geosci., 3, 221–229, 2001 (in Chinese with English abstract).

Imbellone, P. A.: Classification of Paleosols, São Paulo, UNESP, Geociências, 30, 5–13, 2011.

Izumi, K., Kemp, D., Itamiya, S., and Inui, M.: Sedimentary evidence for enhanced hydrological cycling in response to rapid carbon release during the early Toarcian oceanic anoxic event, Earth Planet. Sci. Lett., 481, 162–170, 2018.

Jahren, A. H., Arens, N. C., and Harbeson, S. A.: Prediction of atmospheric $\delta^{13}C_{CO2}$ using fossil plant tissues, Rev. Geophy., 46, RG1002, https://doi.org/10.1029/2006RG000219, 2008.

Jenkyns, H. C.: Geochemistry of oceanic anoxic events, Geochem. Geophys. Geosyst., 11, Q03004, https://doi.org/10.1029/2009GC002788, 2010.

Jenkyns, H. C. and Clayton, C. J.: Black shales and carbon isotopes in pelagic sediments from the Tethyan Lower Jurassic, Sedimentology, 33, 87–106, 1986.

Jenkyns, H. C. and Clayton, C. J., Lower Jurassic epicontinental carbonates and mudstones from England and Wales: chemostratigraphic signals and the early Toarcian anoxic event, Sedimentology, 44, 687–706, 1997.

Jenkyns, H. C., Jones, C. E., Gröcke, D. R., Hesselbo, S. P., and Parkinson, D. N.: Chemostratigraphy of the Jurassic System: Applications, limitations and implications for palaeoceanography, J. Geol. Soc. London, 159, 351–378, 2002.

Jones, C. E., Jenkyns, H. C., and Hesselbo, S. P.: Strontium isotopes in Early Jurassic seawater, Geochim. Cosmochim. Ac., 58, 1285–1301, 1994.

Kemp, D. B., Coe, A. L., Cohen, A. S., and Schwark, L.: Astronomical pacing of methane release in the Early Jurassic period, Nature, 437, 396–399, https://doi.org/10.1038/nature04037, 2005.

Kenny, R.: A cool time in the Early Jurassic: first continental palaeoclimate estimates from oxygen and hydrogen isotope ratios in chert from Navajo Sandstone carbonate lenses, Utah (USA), Carbonate Evaporite, 32, 45–52, https://doi.org/10.1007/s13146-015-0276-z, 2015.

Kent, D. V., Olsen, P. E., and Muttoni, G.: Astrochronostratigraphic polarity time scale (APTS) for the Late Triassic and Early Jurassic from continental sediments and correlation with standard marine stages, Earth-Sci. Rev., 166, 153–180, 2017.

Korte, C. and Hesselbo, S. P.: Shallow marine carbon and oxygen isotope and elemental records indicate icehouse-greenhouse cycles during the Early Jurassic, Paleoceanography, 26, 1–18, 2011.

Korte, C., Hesselbo, S. P., Jenkyns, H. C., Rickaby, R. E. M., and Spötl, C.: Palaeoenvironmental significance of carbon- and oxygen-isotope stratigraphy of marine Triassic-Jurassic boundary sections in SW Britain, J. Geol. Soc. London, 166, 431–445, 2009.

Korte, K., Hesselbo, S. P., Ullmann, C. V., Dietl, G., Ruhl, M., Schweigert, G., and Thibault, N.: Jurassic climate mode governed by ocean gateway, Nat. Commun., 6, 10015, https://doi.org/10.1038/ncomms10015, 2015.

Li, H. C. and Ku, T. L.: δ^{13}C-δ^{18}O covariance as a paleohydrological indicator for closed basin lakes, Palaeogeogr. Palaeocl., 133, 69–80, 1997.

Li, L. Q., Wang, Y. D., Liu, Z. S., Zhou, N., and Wang, Y.: Late Triassic palaeoclimate and palaeoecosystem variations inferred by palynological record in the northeastern Sichuan Basin, China, Paläontol. Z., 90, 309–324, https://doi.org/10.1007/s12542-016-0309-5, 2016.

Li, W. M. and Chen, J. S.: Discovery and significances of the Jurassic Ziliujing Formation in Tianzhu, Guizhou, China New Techn. Prod., 13, 134–135, 2010 (in Chinese).

Li, X. B. and Meng, F. S.: Discovery of fossil plants from the Ziliujing Formation in Hechuan of Chongqing, Geol. Min. Resour. South China, 3, 60–65, 2003 (in Chinese with English abstract).

Li, Y., Allen, P. A., Densmore, A. L., and Xu, Q.: Evolution of the Longmen Shan Foreland Basin (Western Sichuan, China) during the Late Triassic Indosinian Orogeny, Basin Res., 15, 117–138, 2003.

Li, Y. Q. and He, D. F.: Evolution of tectonic-depositional environment and prototype basins of the Early Jurassic in Sichuan Basin and adjacent areas, Acta Petrol. Sin., 35, 219–232, 2014 (in Chinese with English abstract).

Liang, B., Wang, Q. W., and Kan, Z. Z.: Geochemistry of Early Jurassic mudrocks from Ziliujing Formation and implications for source-area and weathering in dinosaur fossils site in Gongxian, Sichuan province, J. Min. Petr., 26, 94–99, 2006 (in Chinese with English abstract).

Littler, K., Hesselbo, S. P., and Jenkyns, H. C.: A carbon-isotope perturbation at the Pliensbachian-Toarcian boundary: evidence from the Lias Group, NE England, Geol. Mag., 147, 181–192, 2010.

Liu, J. L., Ji, Y. L., Zhang, K. Y., Li, L. D., Wang, T. Y., Yang, Y., and Zhang, J.: Jurassic sedimentary system transition and evolution model in western Sichuan Foreland Basin, Acta Petrol. Sin., 37, 743–756, 2016 (in Chinese with English abstract).

Ma, Y. S., Chen, H. D., Wang, G. L., Guo, T. L., Tian, J. C., Liu, W. J., Xu, X. S., Zheng, R. C., Mou, C. L., and Hou, M. C.: Atlas of Lithofacies Paleogeography on the Sinian-Neogene Tectonic-Sequence in South China, Science Press, Beijing, 162–165, 2009 (in Chinese).

Mack, G. H. and James, W. C.: Paleoclimate and the Global Distriution of Paleosols, J. Geol., 102, 360–366, 1994.

Mack, G. H., James, W. C., and Monger, H. C.: 1 Classification of paleosols, Geol. Soc. Am. Bull., 105, 129–136, 1993.

McElwain, J. C., Wade-Murphy, J., and Hesselbo, S. P.: Changes in carbon dioxide during an oceanic anoxic event linked to intrusion into Gondwana coals, Nature, 435, 479–482, https://doi.org/10.1038/nature03618, 2005.

Mckenzie, J. A. and Vasconcelos C.: Dolomite Mountains and the origin of the dolomite rock of which they mainly consist: historical developments and new perspectives, Sedimentology, 56, 205–219, https://doi.org/10.1111/j.1365-3091.2008.01027.x, 2009.

Meng, F. S. and Chen, D. Y.: Fossil plants and palaeoclimatic environment from the Ziliujing Formation in the western Yangtze Gorges area, China, Geol. Min. Res. S. China, 1, 51–59, 1997 (in Chinese with English abstract).

Meng, F. S., Li, X. B, and Chen, H. M.: Fossil plants from Dongyuemiao Member of the Ziliujing Formation and Lower-Middle Jurassic boundary in Sichuan basin, China, Acta Palaeontol. Sin., 42, 525–536, 2003. (in Chinese with English abstract).

Meng, F. S., Chen, H. M., and Li, X. B.: Study on Lower Middle Jurassic boundary in Chongqing region, Geol. Min. Resour. S China, 3, 64–71, 2005 (in Chinese with English abstract).

Metodiev, L. and Koleva-Rekalova, E.: Stable isotope records (δ^{18}O and δ^{13}C) of Lower–Middle Jurassic belemnites from the Western Balkan mountains (Bulgaria), Palaeoenvironmental application, Appl. Geochem., 23, 2845–2856, 2008.

Mintz, J. S., Driese, S. G., Breecker, D. O., and Ludvigson, G. A.: Influence of changing hydrology on pedogenic calcite precipitation in Vertisols, Dance Bayou, Brazoria County, Texas, USA: implications for estimating paleoatmospheric pCO_2, J. Sedi. Res., 81, 394–400, 2011.

Mo, Y. Z. and Yu, H. Y.: The discovery and its geological significance of dolomite in Ziliujing Groups of Middle and Lower Jurassic Series in Ma'anshan Member, Geol. Guizhou, 10, 110–113, 1987 (in Chinese with English abstract).

Montañez, I. P.: Modern soil system constraints on reconstructing deep-timeatmospheric CO_2, Geochim. Cosmochim. Acta, 101, 57–75, 2013.

Nadelhofer K. J. and Fry B.: Controls on natural nitrogen-15 and carbon-13 abundances in forest soil organic matter, Soil Sci. Soc. Am. J., 52, 1633–1640, 1988.

Newport, R., Hollis, C., Bodin, S., and Redfern, J.: Examining the interplay of climate and low amplitude sea-level change on the distribution and volume of massive dolomitization: Zebbag Formation, Cretaceous, Southern Tunisia, Deposit. Rec., 3, 38–59, https://doi.org/10.1002/dep2.25, 2017.

Parrish, J. T., Hasiotis, S. T., and Chan, M. A.: Carbonate deposits in the Lower Jurassic Navajo Sandstone, southern Utah and northern Arizona, J. Sedi. Res., 87, 740–762, https://doi.org/10.2110/jsr.2017.42, 2017.

Parrish, J. T., Rasbury, E. T., Chan, M. A., and Hasiotis, S. T.: Earliest Jurassic U-Pb ages from carbonate deposits in the Navajo Sandstone, southeastern Utah, USA, Geology, 47, 1015–1019, https://doi.org/10.1130/g46338.1, 2019.

Peng, G. Z.: Assemblage characters of Jurassic dinosaurian fauna in Zigong of Sichuan, J. Geosci., 33, 113–123, 2009 (in Chinese with English abstract).

Peti, L., Thibault, N., Clémence, M. E., Korte, C., Dommergues, J. L., Bougeault, C., Pellenard,P., Jelby, M. E., and Ullmann, C. V.: Sinemurian-Pliensbachian Calcareous Nannofossil Biostratigraphy and Organic Carbon Isotope Stratigraphy in the Paris Basin: Calibration to the Ammonite Biozonation of NW Europe, Palaeogeogr. Palaeocl., 468, 142–161, 2017.

Petrash, D. A., Bialik, O. M., Bontognali, T. R. R., Vasconcelos, C., Roberts, J. A., McKenzie, J. A., and Konhauser, K. O.: Microbially catalyzed dolomite formation: From near-surface to burial, Earth Sci. Rev., 171, 558–582, https://doi.org/10.1016/j.earscirev.2017.06.015, 2017.

Philippe, M., Puijalon, S., Suan, G., Mousset, S., Thévenard, F., and Mattioli, E.: The palaeolatitudinal distribution of fossil wood genera as a proxy for European Jurassic terrestrial climate, Palaeogeogr. Palaeocl., 466, 373–381, 2017.

Pole, M.: Vegetation and climate of the New Zealand Jurassic, GFF, 131, 105–111, https://doi.org/10.1080/11035890902808948, 2009.

Price, G. D., Twitchett, R. J., Wheeley, J. R., and Buono, G.: Isotopic evidence for long term warmth in the Mesozoic, Sci. Rep., 3, 1438, https://doi.org/10.1038/srep01438, 2013.

Qian, T., Liu, S. F., Wang, Z. X., Li, W. P., and Chen, X. L.: Characteristics of the Baitianba Formation conglomerate of Lower Jurassic in the northern Sichuan basin and its constraint to the uplift of the south Dabashan, China Sci. Paper, 11, 2402–2408, 2016 (in Chinese with English abstract).

Rees, P. A., Zeigler, A. M., and Valdes, P. J.: Jurassic phytogeography and climates: new data and model comparisons, in: Warm Climates in Earth History, edited by: Huber, B., MacLeod, K., and Wing, S., Cambridge University Press, Cambridge, UK, 297–318, 1999.

Retallack, G. J.: Adapting soil taxonomy for use with paleosols, Quatern. Int., 51/52, 55–57, https://doi.org/10.1016/S1040-6182(98)00039-1, 1998.

Retallack, G. J.: A 300-million-year record of atmospheric carbon dioxide from fossil plant cuticles, Nature, 411, 287–290, 2001a.

Retallack, G. J.: Soils of the Past–An Introduction to Paleopedology, Blackwell Science Ltd, Oxford, UK, 333, 2001b.

Riding, J. B., Leng, M. J., Kender, S, Hesselbo, S. P., and Feist-Burkhardt, S.: Isotopic and palynological evidence for a new Early Jurassic environmental perturbation, Palaeogeogr. Palaeocl., 374, 16–27, 2013.

Robinson, S. A., Andrews, J. E., Hesselbo, S. P., Radley, J. D., Dennis, P. F., Harding, I. C., and Allen, P.: Atmospheric pCO_2 and depositional environment from stable-isotope geochemistry of calcrete nodules (Barremian, Lower Cretaceous, Wealden Beds, England), J. Geol. Soc., London, 159, 215–224, 2002.

Robinson, S. A., Ruhl, M., Astley, D. L., Naafs, B. D. A., Farnsworth, A. J., Bown, P. R., Jenkyns, H. C., Lunt D. J., O'Brien, C., Pancost, R. D., and Markwick, P. J.: Early Jurassic North Atlantic sea-surface temperatures from TEX86 palaeothermometry, Sedimentology, 64, 215–230, https://doi.org/10.1111/sed.12321, 2017.

Romanek, C., Grossman, E., and Morse, J.: Carbon isotopic fractionation in synthetic aragonite and calcite: effects of temperature and precipitation rate, Geochim. Cosmochim. Ac., 56, 419–430, 1992.

Rosales, I., Quesada, S., and Robles, S.: Primary and diagenetic isotopic signals in fossils and hemipelagic carbonates: the Lower Jurassic of northern Spain, Sedimentology, 48, 1149–1169, 2001.

Royer, D. L.: CO_2-forced climate thresholds during the Phanerozoic: Geochim. Cosmochim. Ac., 70, 5665–5675, https://doi.org/10.1016/j.gca.2005.11.031, 2006.

Sabatino, N., Neri, R., Bellanca, A., Jenkyns, H., Baudin, F., Parisi, G., and Maseti, D.: Carbon isotope records of the Early Jurassic (Toarcian) oceanic anoxic event from the Valdorbia (Umbria-Marche Apennines) and Monte Mangart (Julian Alps) sections: palaeogeographic and stratigraphic implications, Sedimentology, 56, 1307–1328, 2009.

SBG (Sichuan Bureau of Geology): Reports of 1:200 000 Regional Geology Investigations (Profile Qianjiang), 48, 1975 (in Chinese).

SBG (Sichuan Bureau of Geology): Reports of 1:200 000 Regional Geology Investigations (Profile Xuyong), 55, 1976 (in Chinese).

SBG (Sichuan Bureau of Geology): Reports of 1:200 000 Regional Geology Investigations (Profiles Suining, Zigong, Neijiang, Yibin, and Luzhou), 43–50, 1980 (in Chinese).

SBGM (Sichuan Bureau of Geology and Mineral Resources): Geology of Sichuan Province, Geol. Publ. House, Beijing, 730, 1991 (in Chinese with English summary).

SBGM: Lithostratigraphy of Sichuan Province, China Uni. Geosci. Press, Wuhan, 388, 1997 (in Chinese).

Schaller, M. F., Wright, J. D., and Kent, D. V.: Atmospheric pCO_2 perturbations associated with the Central Atlantic Magmatic Province, Science, 331, 1404–1409, https://doi.org/10.1126/science.1199011, 2011.

Sellwood, B. W. and Valdes, P. J.: Jurassic climates, P. Geologist Assoc., 119, 5–17, 2008.

Scotese, C. R.: Atlas of Jurassic Paleogeographic Maps, PALEOMAP Atlas for ArcGIS, volume 4, The Jurassic and Triassic, Maps 32–42, Mollweide Projection, PALEOMAP Project, Evanston, IL, https://doi.org/10.13140/2.1.4850.4321, 2014.

Slater, S. M., Twitchett, R. J., Danise, S., and Vajda, V.: Substantial vegetation response to Early Jurassic global warming with impacts on oceanic anoxia, Nature Geo., 12, 462–467, https://doi.org/10.1038/s41561-019-0349-z, 2019.

Soil Survey Staff: Keys to Soil Taxonomy, Pocahontas Press, Blacksburg, Virginia, 1998.

Steinthorsdottir, M. and Vajda, V.: Early Jurassic (late Pliensbachian) CO_2 concentrations based 5 on stomatal analysis of fossil conifer leaves from eastern Australia, Gondwana Res., 27, 829–897, 2015.

Storm, M. S., Hesselbo, S. P., Jenkyns, H. C., Ruhl, M., Ullmann, C. V., Xu, W., Leng, M. J., Riding, J. B., and Gorbanenko, O.: Orbital pacing and secular evolution of the Early Jurassic carbon cycle, P. Natl. Acad. Sci. USA, 117, 3974–3982, https://doi.org/10.1073/pnas.1912094117, 2020.

Suan, G., Mattioli, E., Pittet, B., Mailliot, S., and Lécuyer, C.: Evidence for major environmental perturbation prior to and during the Toarcian (Early Jurassic) oceanic anoxic event from the Lusitanian Basin, Portugal, Paleoceanography, 23, PA1202, https://doi.org/10.1029/2007PA001459, 2008.

Suan, G., Mattioli, E., Pittet, B., Lécuyer, C., Suchéras-Marx, B., Duarte, L. V., Philippe, M., Reggiani, L., and Martineau, F.: Secular environmental precursors to Early Toarcian (Jurassic) extreme climate changes, Earth Planet. Sci. Letts., 290, 448–458, https://doi.org/10.1016/j.epsl.2009.12.047, 2010.

Suchechi, R. K., Hubert, F. F., and Birney de Wet, C. C.: Isotopic imprint of climate and hydrogeochemistry on terrestrial strata of the Triassic-Jurassic Hartford and Fundy rift basins, J. Sediment. Petr., 58, 801–811, 1988.

Talbot, M. R.: A review of the palaeohydrological interpretation of carbon and oxygen isotopic ratios in primary lacustrine carbon-

ates, Chem. Geol. (Isotope Geoscience Section), 80, 261–279, 1990.

Tanner, L. H. and Lucas, S.: The Whitmore Point Member of the Moenave Formation: Early Jurassic Dryland Lakes on the Colorado Plateau, Southwestern USA, Volum. Jur., 6, 11–21, 2008.

Tanner, L. H., Hubert, J. F., Coffey, B. P., and McInerney, D. P.: Stability of atmospheric CO_2 levels across the Triassic/Jurassic boundary, Nature, 411, 675–677, 2001.

Them II, T. R., Gill, B. C., Caruthers, A. H., Gröcke, D. R., Tulsky, E. T., Martindale, R. C., Poulton, T. P., and Smit, P. L.: High-resolution carbon isotope records of the Toarcian oceanic anoxic event (Early Jurassic) from North America and implications for the global drivers of the Toarcian carbon cycle, Earth Planet. Sci. Lett., 459, 118–126, 2017.

Tramoy, R., Schnyder, J., Nguyen, Tu T. T., Yans, J., Jacob, J., Sebilo, M., Derenne, S., Philippe, M., Huguet, A., Pons, D., and Baudin, F.: The Pliensbachian-Toarcian paleoclimate transition: New insights from organic geochemistry and C, H, N isotopes in a continental section from Central Asia, Palaeogeogr. Palaeocl., 461, 310–327, 2016.

Tucker, M. E.: Sedimentary rocks in the field – a practical guide (4th ed.), Wiley-Blackwell, Chichester, England, 276 pp., 2011.

Vandeginste, V. and John, C. M.: Influence of climate and dolomite composition on dedolomitization: insights from a multi-proxy study in the central Oman Mountains, J. Sediment. Res., 82, 177–195, https://doi.org/10.2110/jsr.2012.19, 2012.

van de Schootbrugge, B., Bailey, T. R., Katz, M. E., Wright, J. D., Rosenthal, Y., Feist-Burkhardt, S., and Falkowski, P. G.: Early Jurassic climate change and the radiation of organic walled phytoplankton in the Tethys Sea, Paleobiology, 31, 73–97, 2005.

van de Schootbrugge, B., Bachan, A., Suan, G., Richoz, S., and Payne, J. L.: Microbes, mud, and methane: Cause and consequence of recurrent Early Jurassic anoxia following the end-Triassic mass-extinction, Palaeontology, 56, 685–709, 2013.

Vasconcelos, C., McKenzie, J. A., Bernasconi, S., Grujic, D., and Tien, A. J.: Microbial mediation as a possible mechanism for natural dolomite formation at low temperatures, Nature, 377, 220–222, 1995.

Veizer, J., Godderis, Y., and François, L. M.: Evidence for decoupling of atmospheric CO_2 and global climate during the Phanerozoic eon, Nature, 408, 698–701, 2000.

Wang, Q. W., Liang, B., and Kan, Z. Z.: Carbon and oxygen isotopic compositions of lacustrine carbonates of the Early Jurassic Ziliujing Formation in the Sichuan Basin and their paleolimnological significance, J. Min. Petr., 26, 87–91, 2006 (in Chinese with English abstract).

Wang, Y. D., Mosbrugger, V., and Zhang, H.: Early to Middle Jurassic vegetation and climatic events in the Qaidam Basin, Northwest China, Palaeogeogr. Palaeocl., 224, 200–216, https://doi.org/10.1016/j.palaeo.2005.03.035, 2005.

Wang, Y. D., Fu, B. H., Xie, X. P., Huang, Q. S., Li, K., Liu, Z. S., Yu, J. X., Pan, Y. H., Tian, N., and Jiang, Z. K.: The Terrestrial Triassic and Jurassic Systems in the Sichuan Basin, China, in: Contributions to the 8th International Congress odd the Jurassic System, edited by: Sha, J. G., Shi, X. Y., Zhou, Z. H., and Wang, Y. D., Uni. Sci. Techn., China Press, Hefei, Anhui, 1–136, 2010 (in Chinese).

Warren, J.: Dolomite: occurrence, evolution and economically important associations, Earth Sci. Rev., 52, 1–81, 2000.

Wei, M.: Continental Mesozoic Stratigraphy and Paleontology in the Sichuan Basin, People's Publ. House of Sichuan, Chengdu, 346–363, 1982 (in Chinese with English summary).

Wen, W. and Zhao, B.: Stratigraphic character and sedimentary facies of the Ziliujing Formation in the Pujiang-Ya'An area, Sichuan province, J. Stratigr., 34, 219–224, 2010 (in Chinese with English abstract).

Wright, V. P.: Paleosol Recognition: A guide to early diagenesis in terrestrial settings (Chapter 12), in: Developments in Sedimentology, edited by: Wolf, K. H. and Chilingarian, G. V., Elsevier, Amsterdam, the Netherlands, 47, 591–619, 1992.

Xu, W. M., Ruhl, M., Jenkyns, H. C., Hesselbo. S. P., Riding, J. B., Selby, D., Naafs, B. D. A., Weijers, J. W. H., Pancost, R. D., Tegelaar, E. W., and Idiz, E. F.: Carbon sequestration in an expanded lake system during the Toarcian oceanic anoxic event, Nat. Geosci., 129–135, https://doi.org/10.1038/NGEO2871, 2017.

Xu, W. M, Ruhl, M., Jenkyns, H. C., Leng, M. J., Huggett, J. M., Minisini, D., Ullmann, C. V., Riding, J. B., Weijers, J. W. H., Storm, M. S., Percival, L. M. E., Tosca, N. J., Idiz, E. F., Tegelaar, E. W., and Hesselbo, S. P.: Evolution of the Toarcian (Early Jurassic) carbon-cycle and global climatic controls on local sedimentary processes (Cardigan Bay Basin, UK), Earth Planet. Sci. Lett., 484, 396–411, 2018.

Yang, G. L.: Heavy mineral stratigraphy of Mesozoic continental clastic facies in Yaxi area, northern Guizhou, J. Stratigr., 39, 89–96, 2015 (in Chinese with English abstract).

Ye, M. N., Liu, X. Y., and Huang, G. Q.: Late Triassic and Early-Middle Jurassic fossil plants from northeastern Sichuan, Sci. Techn. Press., Hefei, Anhui, 1986 (in Chinese with English summary).

Zhang, X. S., Zhao, B., Tan, M., Zhou, B. Y., and Sun, J.: Stratigraphic Characteristics of Ziliujing Formation, Jurassic Series and Discovery of Dinosaur Footprints in Dafang, Guizhou, Geol. Guizhou, 33, 50–70, 2016 (in Chinese with English abstract).

Zhang, Z. L. and Meng, F. S.: Chapter 2, the Jurassic. In Zhang Zhenlai and Meng Fansong eds. The Triassic-Jurassic Biostratigraphy in Yangtze Gorges (4), Geol. Publ. House, Beijing, 408, 1987 (in Chinese with English summary).